

# POLITECNICO DI TORINO

Master's Degree in Mechanical Engineering



## Politecnico di Torino

Master's Degree Thesis

## **Optimization of process parameters to produce Ti-6Al-2Sn-4Zr-2Mo parts via the Directed Energy Deposition process**

Supervisors:

Prof. Abdollah Saboori

Candidate:

Alberto Villo'

s290505

A.Y. 2024/2025

Xxxxxxxxxx  
XXXXXXXXXX  
XXXXXXX  
xxxxxxxxxxxx

# Index

Abstract.....	7
Chapter 1. Introduction .....	8
1.1 Introduction to Additive Manufacturing.....	8
1.1.1 Working Cycle of Additive Manufacturing.....	8
1.2 Additive Manufacturing Process.....	9
1.2.1 Material Extrusion.....	10
1.2.2 Binder Jetting.....	11
1.2.3 Powder Bed Fusion.....	12
1.2.4 Directed Energy Deposition .....	12
1.2.5 DED vs other technology.....	14
1.2.6 DED vs. other technology for Titanium alloys .....	15
1.3 Pro & Cons .....	17
1.3.1 PROS .....	17
1.3.2 CONS .....	18
1.4 Titanium Overview .....	20
1.4.1 Ti6242 vs Ti64.....	21
1.4.1 Ti6242 Material Application.....	22
1.5 Process Parameter Optimization of Ti6242 .....	23
Chapter 2. Materials and Methods.....	24
2.1 DED Machine .....	25
2.2 Cutting.....	26
2.3 Mounting.....	27
2.4 Grinding and Polishing .....	29
2.5 Stereo Microscope and Optical Microscope .....	30
2.6 Chemical Hatching Process .....	31
2.7 Tomography.....	31
2.8 Hardness.....	32
Chapter 3. Results And Discussion.....	33
3.1 Single Track Analysis .....	33
3.1.1 Parameters Overview .....	33

3.1.2	Microscope Analysis.....	36
3.2	Single Layer Analysis .....	50
3.2.1	Parameters Overview .....	50
3.2.2	Microscope Analysis.....	51
3.3	Single Wall Analysis.....	54
3.3.1	Parameters Overview .....	54
3.3.2	Microscope Analysis.....	55
3.4	Part Sample Production.....	59
3.4.1	Cross Section Analysis.....	59
3.4.2	Tomography .....	65
3.4.3	Chemical etching.....	68
3.4.4	Hardness Test.....	69
Chapter 4.	Conclusion.....	71
Bibliografy .....		72

# Index

Figure 1.1: Schematic workflow of Additive Manufacturing [2] .....	9
Figure 1.2: Metal Extrusion schematic .....	10
Figure 1.3: Binder Jetting Scheme [10] .....	11
Figure 1.4: DED scheme [17] .....	13
Figure 2.1: Mekton Servocut 402-AA .....	26
Figure 2.2: Cutting Pattern of Plates .....	27
Figure 2.3: Presi KM-U mounting resing .....	27
Figure 2.4: Mounted samples.....	28
Figure 2.6: MINITECH 250 SP1 and sand paper disk .....	29
Figure 2.7: Stereo microscope MZ10F by Leica .....	30
Figure 2.8: Optical Microscope DM6 by Leica .....	30
Figure 2.9: Tomograph by Phoenix .....	31
Figure 2.10: Microhardness tester Wilson VH1150 .....	32
Figure 3.1: First Plate Track Parameter .....	34
Figure 3.2: First Plate Track Parameter .....	35
Figure 3.3: Example of tracks with a focus on their extremities .....	36
Figure 3.4: Tracks 1 to 12, 1× resolution.....	37
Figure 3.5: Tracks 1 to 12, 3× resolution.....	37
Figure 3.6: Tracks 13 to 24, 1× resolution.....	38
Figure 3.7: Tracks 13 to 24, 3× resolution.....	38
Figure 3.8: Tracks 25 to 36, 1× resolution.....	39
Figure 3.9: Tracks 25 to 36, 3× resolution.....	39
Figure 3.10: Tracks 37 to 48, 1× resolution.....	40
Figure 3.11: Tracks 37 to 48, 3× resolution.....	40
Figure 3.12: Effect on width for different Power.....	43
Figure 3.13: Effect on heigth for different Power.....	43
Figure 3.14: Effect on width for different velocity .....	44
Figure 3.15: Effect on heigth for different velocity .....	44
Figure 3.16: Cross section analysis tracks 1 to 12 .....	47
Figure 3.17: Cross section analysis tracks 12 to 24 .....	47
Figure 3.18: Cross section analysis tracks 25 to 36 .....	48
Figure 3.19: Cross section analysis tracks 37 to 48 .....	48
Figure 3.20: Plate with single layer analysis and single walls analysis .....	50
Figure 3.21: Top View of Tracks for Single Layer analysis.....	51
Figure 3.22: Cross-section analysis tracks 1 to 6 for Single Layer analysis.....	52
Figure 3.23: Top View of Tracks 7 to 12 for single wall analysis.....	55
Figure 3.24: Top View of Tracks 13 to 18 for single wall analysis.....	56
Figure 3.25: Cross Section view of tracks 7 to 18 for single wall analysis. ....	56

Figure 3.26: Plate with cubes.....	59
Figure 3.27: Schematic Representation of Cube section Zone .....	60
Figure 3.28: images of Cube 1 from optical microscope, superficial porosity calculated through ImageJ .....	61
Figure 3.29: images of Cube 2 from optical microscope, superficial porosity calculated through ImageJ .....	61
Figure 3.30: images of Cube 3 from optical microscope, superficial porosity calculated through ImageJ .....	62
Figure 3.31: images of Cube 4 from optical microscope, superficial porosity calculated through ImageJ .....	62
Figure 3.32: images of Cube 5 from optical microscope, superficial porosity calculated through ImageJ .....	63
Figure 3.33: images of Cube 6 from optical microscope, superficial porosity calculated through ImageJ .....	63
Figure 3.34: Cube 1 Tomography .....	65
Figure 3.35: Diameter vs Volume of pores in Cube 1 .....	65
Figure 3.36: Cube 4 Tomography.....	66
Figure 3.37: Diameter vs Volume of pores in Cube 4 .....	66
Figure 3.38: Cross section of the cube after etching chemical process, under stereomicroscope .....	68
Figure 3.39: Cross section of the cube after etching chemical process, under optical microscope ...	68
Figure 3.40: Schematic Representation of Cube section Zone .....	69

## Abstract

Titanium alloys in the last decades have caught large use in various sectors such as aerospace, biomedical, and motorsport owing to their peerless strength-weight ratio, excellent corrosion resistance, and toughness. The Ti-6Al-2Sn-4Zr-2Mo (Ti6242) enhances further application with respect to the most common Ti-6Al-4V, with a higher maximum temperature of exercise (540°C). However, the machinability of this alloy is demanding, and additive manufacturing (AM) provides a great solution to reduce tool usage, with the possibility of building a complex shape component in layerwise manner instead of subtracting, which is the basic mechanism in traditional technologies. Among the AM technologies, the DED process demonstrated great competence in the production of semi-complex large Ti6242 parts. However, so far, the production of Ti6242 parts via the DED process has rarely been investigated. For this reason, this thesis aims to process this alloy for the first time and find the most suitable combination of process parameters through a stepwise approach, starting from the single scat track analysis followed by single layer, single wall, and cube production. In fact, starting from a family of the most relevant parameters, single tracks are analysed to find the best combination of the laser-related parameters, with single wall and single layer analysis to find the best hatching distance and z-step parameter. At the final stage, cubes as representative parts have been built up and analysed. Finally, cubes undergo cross-section analysis and tomography to evaluate part's final density, while microstructure analysis is detected through chemical etching.

# Chapter 1.

## Introduction

### 1.1 Introduction to Additive Manufacturing

Additive Manufacturing (AM) is a manufacturing technology, whose base principle and terms are defined in ISO/ASTM 52900:2021. A general description can be provided as a generative building process, where the part is built layer by layer, using a source power as heat or fixing source and material can be fed in different ways and standing.[1]

#### 1.1.1 Working Cycle of Additive Manufacturing

The general work cycle can be divided into the following steps[2]:

- **3D CAD creation**

Nowadays, most objects are designed using 3D CAD software. The main advantage of this software with respect to technical drawings is the possibility to edit them and the possibility to study FEM analysis directly on the 3D part. With FEM analysis, Design for Additive Manufacturing could be enhanced, having the possibility to reduce material (and weight) with a cycling optimization loop based on FEM data.

These 2 main reasons have made 3D CAD software the base of the design process for AM but also for traditional technology.

- **STL file conversion**

STL is a file format native of stereolithography CAD software by 3D systems. STL decomposes a 3D CAD into triangles, using a cartesian coordinate system for each triangle's vertices. Furthermore, a vector is associated with the surface orthogonal direction. Even if some information could be lost during conversion (as material, colour, etc., etc.) and even if triangle approximation may lead to inaccurate geometry, STL format is the most used due to its easy generation process and data processing, both during writing and reading of STL part files.

- **STL slicing**

Slicing is the process where the STL file previously created is now "sliced" layer by layer. The slicing process allows for the creation of a code that control machine tools, or in the AM, the path of

the laser or nozzle to create the slicing plane. In this step, the first optimization is made for the print layout, part orientation and all drawbacks related to the printing phase.

- **Printing of the sliced part**

Before printing, parameters should be optimized. Depending on the technology used, they could be different. Furthermore, material is also a main factor for parameter choice for each technology.

- **Post Processing**

The post-processing and the printing steps depend on the type of process used and the application of the printed part. For the metal additive manufacturing (MAM) fields of application, there are several, biomedical [3] and aerospace are two of the main [4], and depending on the field, different post-processing could be used. A deeper detail on post-processing will be explored in a later paragraph.

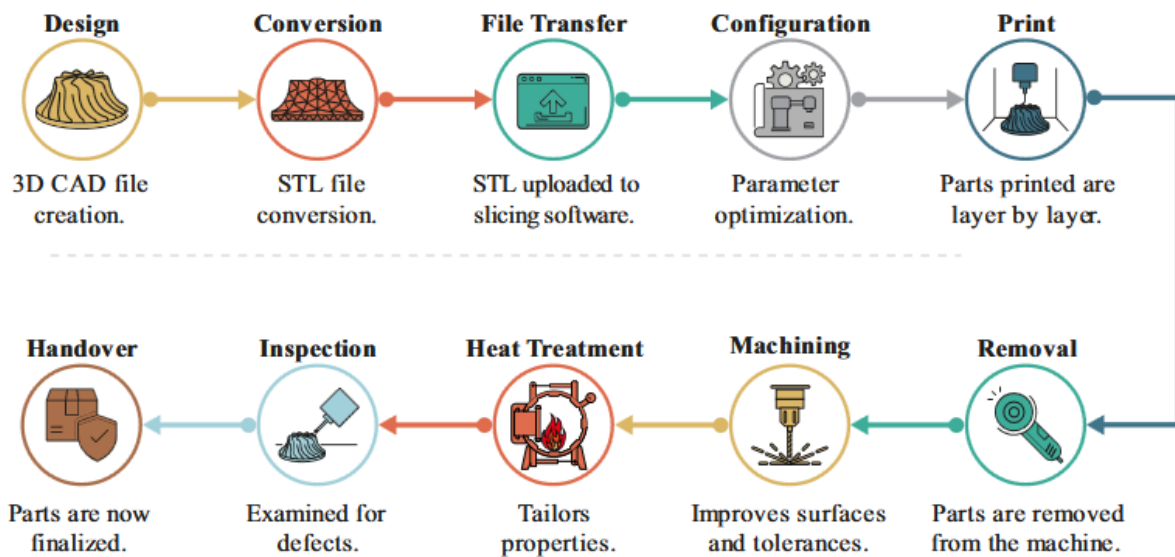


Figure 1.1: Schematic workflow of Additive Manufacturing [2]

## 1.2 Additive Manufacturing Process

In the ISO/ASTM 52900:2021, seven classes of additive manufacturing processes are defined as follows with a brief description [1]:

- Sheet Lamination -> sheet of metal joined by welding.
- VAT polymerization -> liquid photopolymer, with a UV energy source that solidifies components layer by layer.
- Material Jetting -> Polymers or waxes are deposited in drops, and a UV energy source solidifies them.
- Binder Jetting -> powder is deposited on the building platform, and a print head deposits the binder adhesive locally on top of the powder where required.
- Directed Energy Deposition -> powder is deposited directly from the nozzle, where an energy source melts it directly after material spillage from the nozzle head.
- Material Extrusion -> material passes through a nozzle where it is heated, extruded, and deposited layer by layer.
- Powder Bed Fusion -> powder is deposited on a building platform, and an energy source melt or sinters the material selectively.

According to these classes, material and energy sources are the main factors characterizing AM technology. From these only the last four classes use metal materials. For the purpose of this work, a more detailed overview of Metal Additive Manufacturing technology (MAM) will be given in the next paragraphs, with a particular focus on DED.

### 1.2.1 Material Extrusion

Material Extrusion (ME) was born from Fused Deposition Modelling (FDM), and currently takes 10% of the AM market due to its economicity and versatility.[2]

The material, polymers or polymers matrix with metal, are extruded by a nozzle, which is in charge of melting or heating up the material to make deposition possible. The material is deposited layer by layer, following the path generated during the slicing process. A schematic representation is reported in “Figure 1.2”.

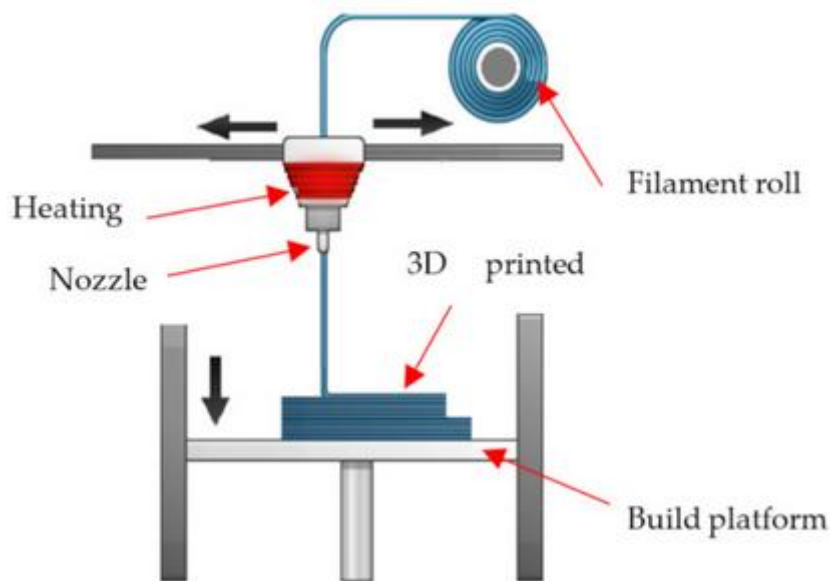


Figure 1.2: Metal Extrusion schematic

For metal or ceramic materials, whose melting temperature is higher with respect to polymer, the metal powder is bounded in a polymer matrix. The polymer is then heated up to melt and deposited layer by layer. [5], [6], [7] During deposition, to easily remove support, a ceramic layer is deposited over the support structure.

The as-build parts are made of the following components [8]:

- Core
- Backbone
- Metal particles
- Ceramic particles
- Additives

In the first debinding stage, the core and additives components slowly degraded. The core is usually made of a dissolvable material that can undergo catalytic degradation. After the full degradation of the core, the remaining part is named “brown” part. The brown part is made of metal and backbone.

This latter has the aim to strengthen the part. The last stage is the sintering. During the sintering process, the brown part is heated to a temperature around 70-90% of metal melting temperatures. During the early stage of sintering, the backbone dissolves, retaining only metal and ceramic particles in place. Metal particles increase with heat, generating bonds and necks between each other. Sintering is crucial for printing results since it's the main responsible for porous presence [8].

As the last paragraph states, the most crucial point for this technology is post-processing and the capability of bounding one layer and layer over it. The layer's adhesion is enhanced by additives, but it is still the weakest strength direction of the part. Thermal stresses are generated during all post-processing and due to material shrinkage, the possibility of cracking or detachment of the part is high if the temperature is not deeply controlled and investigated.

The layer-by-layer building process makes the part intrinsically anisotropic, and this diversity between directions could be softened by an accurate post-process. So, post-processing in this case and in other technology, as following paragraphs will report, is crucial for result, and must be considered as an integer part of the additive process.

### 1.2.2 Binder Jetting

Binder Jetting technology, BJ, is based on a bed of metal powder on which the print head pour a liquid binder, a photopolymer. The printing usually takes place at ambient temperature, and due to its nature, the printed part doesn't need support. [9]. A representation is shown in

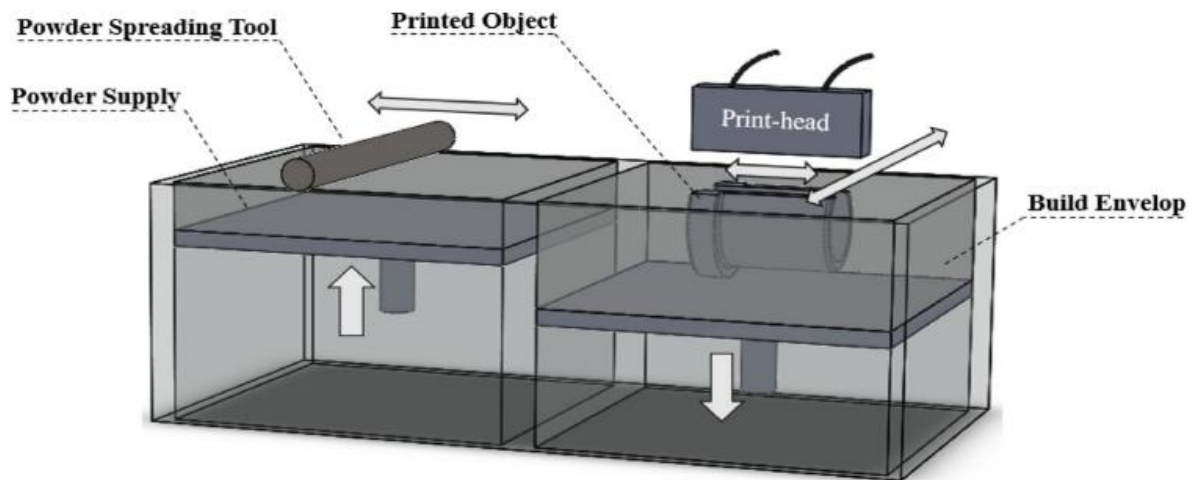


Figure 1.3: Binder Jetting Scheme [10]

The liquid binder takes room between the metal particles of the powder, fulfilling voids. After pouring, a UV light passes over the layer, curing the binder and giving it the strength to support the metal particles. [11]

The excess powder is eliminated by washing and then the part is heated up to the sintering temperature. In this phase, the binder evaporates, while the metal sintering process starts, decreasing the metal porosity of the whole part. The increasing temperature accelerates grain boundary growth and necking between particles. Other than this, the sintering process improves mechanical properties.[12]

As in the previous paragraph, one of the main drawbacks is the shrinkage of the material. This phenomenon leads to residual forces entering the part that could result in distortion of the part or layer separation. For this reason, all the sintering processes and post-processing should be deeply analysed, focusing on temperature and temperature growth rate, to void the possibilities of residual thermal forces and part breaking.[11]

### **1.2.3 Powder Bed Fusion**

Like BJ, the powder bed fusion, PBF, uses a bed of metal powder, but this latter is melted in situ with thermal energy focused on the powder. Thermal energy could come from different energy sources, laser and electron beam are widely used in nowadays technology. [13]

As BJ also, this technology doesn't need support for the part that is self-sustaining by the powder, but in this case, the temperature reached by the powder is higher since focus of thermal energy leads to the melting of the powder itself. The melting leads to some major drawbacks. The first one is about powder oxidation. An inert gas is inflated in the chamber once air is removed to reduce this phenomenon. Usually, argon or helium are the most used gas. [14]

Second is thermal stress; in this case, stresses generated are not during post-processing but during part building. This could lead to detachment from the building plate or from layer to next, without an accurate part or, worst case to cracking of the part itself. To smooth this phenomenon, usually the chamber is heated up to a preheating temperature, reducing the thermal stress between melted powder and the layer previously deposited. [15]

### **1.2.4 Directed Energy Deposition**

For Directed Energy Deposition technology, DED, the description will be more accurate, since it's the main technology used in this work.

DED could be described as a CNC printing head, in which both materials and energy sources join; the energy source melts the metal, and with the CNC head path on a building plate, the building part raises layer by layer. The table could be turntable to further increase printing direction. [16]. A schematic representation is reported in "*Figure 1.4*".

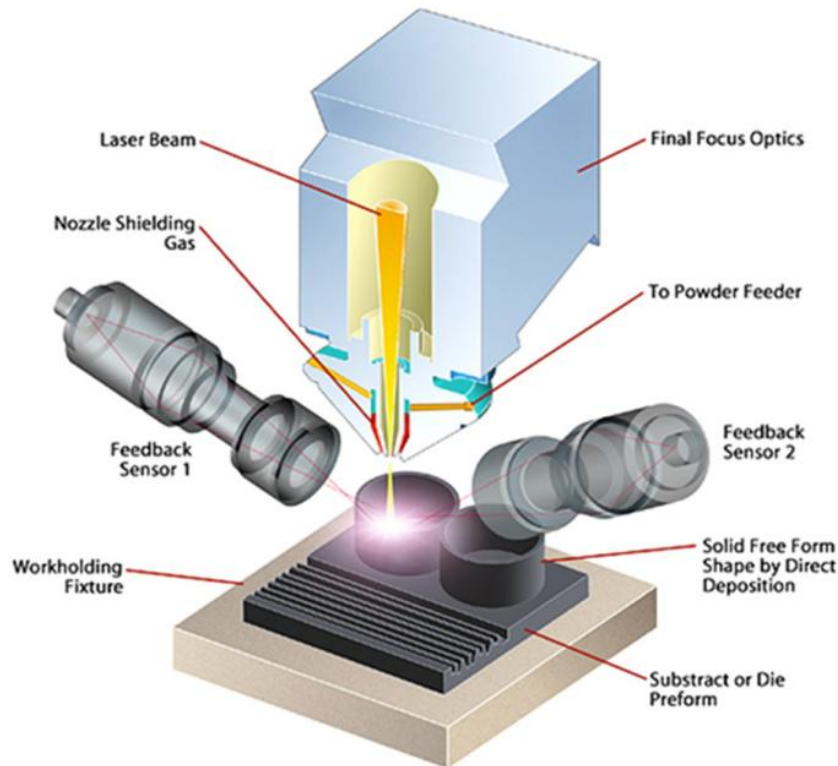


Figure 1.4: DED scheme [17]

As in PBF, the energy source could be of a different nature, mainly plasma laser, electron beam, electric arc, and laser beam. The material used could be either wire or powder, so many commercial welding and powder metallurgy materials are free to be used. The chamber is not fixed since the material is directly fed to the printing head. This allows DED to be more versatile, with no limit to small chamber like other technologies. A gas shield to avoid oxidation is possible in situ of printing material[18]. According to the choice of material, energy source, and printer company ,different names have been addressed to DED [19]:

- LWAM laser welding additive manufacturing.
- WAAM wire arc additive manufacturing
- GMAW gas metallic arc welding,
- PAW plasm arc welding.
- GTAW gas tungsten arc welding
- LDMD laser directed metal deposition
- LMD laser metal deposition
- DMD directed metal deposition
- LSF laser solid forming
- DLF directed light fabrication
- EBAM electron beam additive manufacturing.
- LENS laser engineered net shaping.

Each of them is characterized by different energy sources and different types of material. Another difference between DED technology is the possibility of having a chamber that is not limited. By the nature of the technology, since melting and material are both fed directly in situ of printing, the bed could not be limited to a sized chamber like other technology, even if some of them still have a limited chamber as other technologies[16], [19]. The possibility of having a chamber that is not delimited, is a major advantage with respect to other MAM technologies. This allows for the making of bigger parts and enhances the possibility to repair existing parts. The drawback is the difficulty in analysing and clearly defining in the space the existing part, avoiding collision with the head printer and controlling the temperature between subsequent layers. Due to the open chamber, preheating of the powder is not possible, and the temperature gradient is higher with respect to other technologies that allow preheating. For this reason, DED technologies need further effort in defining process parameters to mitigate thermal effects like roughness and residual stress on finished built parts.

The characteristic of an open chamber and a printing head enhance the possibility of hybrid manufacturing or subtractive hybrid manufacturing. Since the process is like CNC machining, the printing head could be exchanged with a CNC subtractive tool as a milling tool or rolling tool.[20] The possibility of exchanging the printing head gives a major advantage in surface finishing and finishing of hidden surfaces, which are all surfaces that are not post-processable after the end of the printing process[20]. Furthermore, with rolling, it is also possible to change the mechanical properties based on the mission of the printing parts. In some printed parts, this aspect allows the possibility of avoiding post-processing, making the whole part process in just one working station. Even if the advantages are evident with hybrid manufacturing, path controlling and tool change are more difficult to include in the existing complex process parameters control [21]. Another aspect to consider during the process is the need to foresee or monitor thermal distortion of previous layers, which can lead to tool collision and damages of both parts and tools themselves. Last, monitoring the previous layer, mainly temperature state, is crucial for determining when to subtract material with the CNC tool; for this reason, an adaptive strategy for machining must be implemented, considering the status of the layer during the time[20], [21].

The last difference with respect to other MAM technologies is the possibility of DED to have powder mixed directly into the printing head. This procedure has not been studied in detail since control one powder is still a big challenge in modern studies. Still, with two “compatible” powders, the possibility of changing them during part printing, or their ratio allows the parts to have multi-material properties or functional graded materials based on needed and mission of the part itself [22]. However, multi-material parts need predictive capabilities, advanced machine learning and in situ monitoring with adaptive control techniques, and adaptive process parameters to fulfil the multi-material mission. A limitation of this material is the large anisotropy in mechanical properties, and the impossibility of having a homogeneous thermal post-processing since a thermal cycle will affect different parts of the printing in different ways. The possibility of mixing alloys gives DED a suitable mission for testing new materials. In a relative short period of time, is possible using it, to create samples and test the mechanical properties of new alloy[22], [23].

### **1.2.5 DED vs other technology**

Based on what has been reported in the previous paragraph, the main metal additive manufacturing used nowadays are Selective Laser Melting (SLM), Electron Beam Melting (EBM), which both are

based on the Powder Bed Fusion (PBF) category, and Directed Energy Deposition (DED). The main difference between these is the melting powder moment. In the PBF ones, the melting pool is in the bed, while in DED, the powder is melted directly in the deposition locus. The EBM technology requires a vacuum environment, while the laser and direct energy deposition rely on the inert atmosphere. Due to this requirement, EBM need a closed chamber that can be heated up, and the the SLM technology needs a closed chamber for powder deposition. Instead, the DED technology doesn't need a closed chamber since the deposition of the powder happened through the deposition head, allowing DED technology to have a potential not closed chamber. On one hand, SLM and EBM have the possibility to heat up the chamber, reducing the residual stress on the parts, but the part must be of limited size; on the other hand, DED technology has the possibility to have a higher deposition chamber but operating at ambient temperature, the temperature gradient during deposition creates higher residual stress. The size of the chamber also has a major role in accuracy. PBF technologies have higher accuracy, surface finishing, but also higher building rate.

In order to have a general comparison and overview of the 3 technologies taken in consideration a summary has been reported in “Table 1.1” while in chapter “151.2.6 DED vs. other technology for Titanium alloys”, a deeper focus on Titanium alloys has been given

Table 1.1: DED vs SLM vs EBM

	DED [24], [25], [26]	SLM [27], [28], [29]	EBM [30]
Energy Source	Nd-YAG or CO <sub>2</sub>	Fiber Laser	Electron Beam Source
Power	Up to 10000W	Up to 1000W	Up to 3500W
Shielding Gas	Local He/Ar	Chamber He/Ar	Chamber Vacuum + He/Ar
Building Size	Unlimited	As for chamber	As for chamber
Pre-Heating	Unavailable	Up to 200°C	Up to 1000°C
Accuracy	Up to 0.5 mm	Up to 0.05 mm	Up to 0.2 mm
Layer Thickness	Up to 100 microns	Up to 20 microns	Up to 50 microns
Surface Finish	Up to 20 micorns	Up to 5 micros	Up to 15 microns
Building Rate	Up to 200 cm <sup>3</sup> /h	Up to 50 cm <sup>3</sup> /h	Up to 100 cm <sup>3</sup> /h

### 1.2.6 DED vs. other technology for Titanium alloys

In the next chapter, a deeper detail on Titanium and its alloys will follow. However, for the purpose of the thesis, a comparison of the main differences between DED technology and PBF technology could support a deep understanding of the main differences.

In the literature, the widest-used Ti alloys is definitely the Ti64 alloy, while the Ti6242 is not so used. Anyway, to understand the main difference, Ti64 represents a good example due to its similarity with Ti64.

Generally speaking, the tensile properties of the Ti alloys produced via AM technologies are comparable with those of traditional ones [31]. The EBM is generally among the AM technologies with lower tensile properties but still comparable with traditional ones. Instead, the SLM and DED technologies show higher tensile properties but lower ductility [32]. This behaviour could be

addressed by the different microstructures of the alloy related to different temperatures during the process and during the solidification of the part.

Another mechanical characteristic relevant to the usual titanium application is fatigue life. A crucial factor for fatigue is porosity. As reported in the following chapter, several factors determine porosity on the AM part, and due to the process nature using powder, some inclusion, lack of fusion, or gas pores may occur. In the literature, SLM has been considered as the technology with the lowest lack of fusion (0.08% with optimized process), followed by EBM (0.25%) and DED (0.5%). To reduce this factor, some postprocessing is possible, such as high isostatic pressure. Pores create a lower section resistance and the possibility to enhance crack propagation. Similar behaviour applies to surface roughness, if this latter is poor, crack propagation and initialization are more likely to happen on a rough surface.

DED is the one with better surface roughness, followed by SLM and EBM. [32] Finally, residual stresses are a significant factor in fatigue properties; the layer-by-layer process, with local melting of the powder, creates high-temperature gradient and high residual stress. Furthermore, due to the scan strategy high anisotropy is present on the same part, making the behaviour unpredictable. For the EBM process, thanks to the possibility of heating up its chamber, the residual stresses are lower than SLM and DED. This is reflected into a higher fatigue toughness for EBM (up to 5 MPa) followed by DED (up to 3.5 MPa) and SLM (1.7 MPa); however, due to microstructure created in SLM and DED with a higher cooling rate, the fatigue strength is usually higher (500 MPa) than EBM (350 MPa) [32]. In “*Table 1.2*” a summary of what is reported in paragraph

Table 1.2: Summary of Ti64 properties for DED, SLM and EBM technologies.

	DED	SLM	EBM
Yield Strength [MPa]	950	980	900
Ultimate Strength [MPa]	1000	1100	900
Roughness	Up to 0.1	Up to 0.1	Up to 0.3
Fatigue Toughness [MPa]	Up to 3.5	Up to 1.7	Up to 5
Fatigue Strength [MPa]	500	550	350

## 1.3 Pro & Cons

After this overview of all AM technologies, to better understand the potentiality, major pros and cons will be reported in the next paragraph. This will be just an overview of them, but to fully understand the advantages and drawbacks a deeper focus is needed, and a distinction of application case by case should also be taken into account.[23]

### 1.3.1 PROS

Starting from the so-called "Complexity for free", this is the possibility with AM technologies to have a geometry that usually can't be reached with traditional technologies or that its production is expensive with traditional technologies[33]. Even if feasible, a complex geometry with traditional technologies will lead to a multi-step production, while for AM technologies an increase in complexity will not generate an increase in production time. Furthermore, also internal closed geometry is generally possible on AM technologies, where internal channels are created during printing; these are not generally feasible in post-machining for parts with traditional technologies [34].

Since increasing complexity will not affect the production time, AM parts can be produced in a shorter time with respect to traditional ones. However, at today's availability of technologies, mass production, and big parts production are still limited by small and fixed chambers. [34]

The complexity certainly affect the shorter production time; however, this feature also applies to proto parts. Taking for example casting or forging, to have a part produced, a lead time in tool design and build, is for sure longer than the lead time in file preparation and printing.[34] With the same example, the characterization of new material is also easier in AM technologies, for the possibility of easily changing the feed material. Moreover, some materials have low machinability, requiring special tools or special machining conditions; even for low-machinable materials, characterization through additives could be a solution and a fast way to achieve results. Multilaterals are instead a key peculiarity of AM technologies since, with traditional ones, selective anisotropy is not feasible[34], [35].

With AM built parts, generally, the roughness is higher than that of traditionally manufactured parts. Nevertheless, for many applications, a refinement in roughness is not needed, decreasing the overall time for part production[36]. For some applications, instead, only the coupling zones need to have a refined roughness, or tolerance zone that is not reachable directly with as-built parts. So, depending on the application, it is possible to have the final part in only one process, reducing the process to time cost[37]. Also, the inventory needed to print the part is limited compared to the technology used in manufacturing. If an as-built part is suitable for the application, feedstock material is the only inventory needed. [36], [37]

Another peculiarity of the AM is the possibility of mass reduction. With complexity for free, the optimization off low-stress zones could be optimized with few constrain for production with respect to traditional technologies[38]. Furthermore, some peculiar structures such as lattice ones, can be implemented to reduce the mass. A lattice structure is a repetition in the space of an elemental cell whose geometry allows it to have a linked overall part with a wanted void inside. This gives the

possibility to have lighter parts; Nevertheless, the mechanical behaviour of this structure is hard to predict.[39], [40]

Finally, the AM technologies give the possibility to minimize the waste of unneeded materials, to have lighter parts, which on vehicles leads to lower emissions, and for some applications the possibility of having the whole part manufactured in one step, saving energy and time[41], [42]. To have a better overview of the possibilities for an AM built part to save energy, the whole part life should be taken into consideration, also based on the evolution of the market request and availability of feed stock material. As a general rule, AM represents one of the most suitable production technologies for low volume market and high complexity parts.

### 1.3.2 CONS

To have an overview of the main cons, it's helpful to go deeper into the main process. For MAM technologies, the process could be divided as follows:

- Machine state monitoring: data acquired directly or indirectly during printing.
- Powder or wire feed monitoring
- Melt pool monitoring
- Post-processing
  - o Shot peening or sandblasting or removing excess powder
  - o Support removing for technologies that need them
  - o Heat treatment for stress relieving, changing mechanical properties reducing porosity and having a more homogeneous structure
  - o Secondary machining, like CNC, is used for all the zones that need higher precision (for example, coupling zones), or to reduce roughness and raise fatigue mechanical properties.

The first three steps are controlled by setting parameters on the machine, which represent one of the main critical aspects of MAM. [43], [44]

Starting from the machine parameters, the main relevant ones are energy output, scan speed, material federate, and laser spot focus (if present). To a minor extent, but still relevant are hatching and z step. Each material and each technology have its own parameters to produce a good result in part printing. Find them is still a challenge and matter of study for companies and utilizers.[44]

During the process, these parameters are usually considered as constant, except for the first layers that could have a dedicated strategy. Most recently some adaptive strategies are used, with which, during the process, parameters change and adapt themselves based on printing conditions[45]. These printing conditions are taken with state monitoring of the process. With feedback from the actual state, the main process parameters could be changed. The state monitoring could be direct, with a thermal camera, sensor or indirect, combining direct quantities.[46]

Apart from main quantities, also printing strategy could lead to completely different results. In particular, direction of printing, superposition of layer are the main affecting the final results. [43], [44]

During printing process, some major defect could appear. In particular, two between the most common are cracking, and delamination, both mainly caused by thermal residual stress raise [47]. Delamination is the detaching of two subsequent layers, which is caused when the thermal stress is higher than the yield strength of the material. [48] Cracking instead appears when the local thermal stress is higher than the ultimate strength of the material.[49] During solidification, cracking or delamination could be caused by higher contraction of the material due to a higher temperature relative to the previous layer. Cracking could also happen during the liquid phase, during rapid heating or cooling, creating precipitation of the material and contraction. This latter is mainly of alloys with higher differences between solid and liquid phase, or high shrinkage during changes of phases. To mitigate these phenomena, a pre-heated material is possible in fixed chamber technologies or a change in material composition to have better thermal change behaviour.[47], [48], [49]

Another common defect that is present in parts created with MAM technologies is porosity. This is the presence of some void in the total structure of the part. Mainly 2 types of porosity are present[50], [51]:

- Keyholes, generated by high energy density during deposition with gas entrapment, pores are elongated and in building direction
- Gas porosity from feedstock material, with selective evaporation of an element or inclusion of the shielding gas, pores are smaller than keyholes and are mainly spherical
- Lack of fusion, when the energy is not sufficient to fully melt the material, is the largest void between porosity and irregular.

These 3 kinds of porosity could also be characterized by the sphericity of the voids, in particular low spherical are addressed to porosity (0.6), medium spherical correspond to keyholes (0.7) and the most spherical are usually gas porosity (0.92). [50], [51]

To individuate this characteristic, density is the key factor, higher it is, less voids and porosity are present, as an example, Archimedes method, X-ray, tomography, and image analysis of cross-section, are all methods to identify a potential porosity inside the part. The main parameters who affect porosity are powder feed rate, energy source, and laser scan speed. Porosity is a direct factor of fatigue resistance, anisotropy, and corrosion resistance. It is well documented that the porosity can affect the mechanical properties of the printed parts make them not reliable.[51]

Roughness is another KPI to monitor in MAM technology. If the process parameters are not optimized, a poor surface roughness could appear. This effect is mostly for unmelted powder that sinters to the surface during the process, creating the external rough layer.

Roughness is one of the key factors in fatigue analysis and corrosion resistance since poor roughness could enhance crack propagation. [37], [45]

## 1.4 Titanium Overview

Titanium is a widely used element, that is peculiar for its high specific strength, fracture toughness, fatigue, and corrosion resistance[52]. For these properties it's one of the most suitable metals for biomedical applications since it's highly biocompatible, and for aerospace applications.

However, it's one of the most difficult materials to be machined and has a high purchasing cost. For this reason, AM technologies, with as-built parts and low scrap material, are suitable for AM part production.[53]

Titanium has 2 stable phases[54]:

Phase Alpha,  $\alpha$ , hexagonal close packed HCP

Phase Beta,  $\beta$ , body centered cubic BCC

Then, some metastable phases are also present[54]:

$\alpha'$  – from  $\beta$  phase with water quenching

$\alpha''$  - from  $\beta$  phase with water quenching

$\beta'$  – with rapid cooling and  $\beta$  stabilizer elements

$\omega$  – with rapid cooling and  $\beta$  stabilizer elements[55]

These phases depend mainly on the production process and composition of the alloy.

Each titanium alloy has a Beta-transus temperature, in which the beta phase transforms into alpha. This temperature is affected by alpha-stabilizing elements, like AL, O, N, and C, and others are beta-stabilizing elements, like Mo, V, Cr, Fe, Mn, Nb, and Ta.

The Beta-transus temperature in literature has been modeled several times, and the formula changes the T value on the amount of weight element, lowering it if it's an alpha stabilizer or increasing the temperature with beta stabilizing elements.[56].

During AM part building, particularly in DED technology, the heat gradient between the chamber and melting temperature is high, with fast heating dissipation. This leads to a prior beta columnar grains formation, while the alpha phase is more nucleated at the boundary of the prior beta grains. However, different phases could happen between subsequent layer or in the same layer due to the thermal differences between the bottom of the melting pool and the upper part. [57]

A thermal post-process cycle is used to solve the microstructure anisotropy of the titanium or to search for a defined microstructure. [55]

Thermal process, due to changes in microstructure, highly affects mechanical properties. In the as-built part, because of the rapid cooling rate and induced fine microstructure, the strength is higher while the ductility is lower. The mechanical properties reflect the anisotropy microstructure, with different properties for different directions. Furthermore, the beta phase exhibits a higher strength, with low ductility and the presence of alpha at the grain boundaries reduces the elongation. [58], [59] In the thermally treated parts, the precipitation of alpha phases decreases the strength, increasing ductility, and with targeted modification of microstructure, different levels of strength and ductility could be reached. The two main factors in charge of the microstructure modification are heating temperature and cooling rate. [58], [59]

Another main propriety that characterizes titanium is high fatigue resistance. However, it mainly depends on crack nucleation and propagation in the part. Crack nucleation could be worsened by poor surface roughness, while crack nucleation is affected by pores and impurities in the part. [60]. As stated in the previous paragraph, both porosity presence and poor surface roughness are present in the AM built part. While poor surface roughness could be diminished by post machining, a deep study of process parameters optimization should be undertaken for porosity [61]. The fatigue resistance could be further increased with the aimed microstructure. As a general state, alpha and alpha' microstructure increase fatigue strength resistance but lower ductility.

### 1.4.1 Ti6242 vs Ti64

The most used titanium alloy in the market is the Ti64. However, some other alloys have different properties and are used for different applications. Between them, Ti6242 is one of the latest considered.

Ti6242 and Ti64 show the following composition [62]

Ti-6Al-2Sn-4Zr-2Mo:

- 6% Aluminium (Al)
- 2% Tin (Sn)
- 4% Zirconium (Zr)
- 2% Molybdenum (Mo)
- 86% Titanium and other minor elements

Ti-6Al-4V:

- 6% Aluminium (Al)
- 4% Vanadium (V)
- 90% Titanium and other minor elements.

Ti64 is classified as an Alpha-Beta alloy, with Aluminium stabilizing the alpha phase and vanadium beta one. Ti6242 is a near-alpha alloy, with a smaller amount of beta phase [63]. The alpha phase in this alloy is stabilized by aluminium and tin, while the beta is stabilized by zirconium and molybdenum. However, the composition of Ti6242, has the peculiarity of enhancing the stability and performance of the alloys at high temperatures.[55]

Ti64 and Ti6242 show similar mechanical properties, with Ti6242 having slightly higher Tensile Strength and Yield Strength. Both have good ductility, but Ti6242 has better ductility at high temperatures, as well as higher fatigue resistance at higher temperatures. [63], [64], [65]

However, Ti6242, due to its near alpha structure, it's less machinable and weldable with respect to Ti64 [65]. For this reason, AM technologies are one of the most suitable production technologies, since there is no machining in the part, specifically when as-build conditions are suitable. [66]

### **1.4.1 Ti6242 Material Application**

As the previous section, titanium alloys are the of the best for their good strength-to-weight ratio, toughness, and corrosion resistance. Ti6242, added to the previous, also has a good resistance at medium-high temperatures, making it suitable for aerospace components such as aero-engine compressors, impellers and power generators [67]. The same properties are also needed for high-performance cars, such as turbines, engine components, anti-roll bars, and damper spring.

Another difference with respect to the usual Ti64 is the absence of Vanadium, making the Ti6242 a more suitable solution for the biomedical field [68]. During biomedical implants, there is the possibility of the oxide layer being damaged, and metal ions can be released in the blood stream. Even if, to a minor extent on Ti64, some vanadium oxides could be found on the surface of the implants, these are cytotoxic for humans.[68] Instead, the Ti6242 doesn't have Vanadium in this composition, making it more suitable for implants, having all the advantages of titanium alloys for implants and of additive manufacturing technologies, such as the possibility to have porous or lattice structure to make prosthesis lighter, with a density closer to the human bones.

Despite the high proprieties, the titanium alloys generally have low machinability, and Ti6242 is even less machinable than Ti64. In additive manufacturing, the part has the possibility to be deposited as similar as possible to the final part, reducing the machining zones to the only needed. However, the usual porosity that could be found in additive manufactured parts and its low predictability doesn't match the aerospace requirements since it is a critical factor for fatigue resistance.

## 1.5 Process Parameter Optimization of Ti6242

From previous paragraphs, it is possible to understand why additive manufacturing is one of the most suitable technologies for Ti6242. The most challenging part of additive manufacturing production is optimizing process parameters.

Process parameter optimization is needed at first to successfully build the part, but a refinement in optimization is needed to reduce as much as possible defects.

Different approaches are possible, with different aims. In the recent decades, in-situ optimization, with adaptive strategies, has shown high potential in parts creation [69].

This kind of optimization needs a high level of process modelling, with both real-time monitoring acquisition and state predictions. Modelling is nowadays the hardest challenge to face since the parameters are multiple and influence each other [70]. One of the most important differences between other process optimization is the possibility, in case of adaptive strategies, of correcting defects during the process. In this way, the whole optimization process is faster, and geometry and internal defect are lower compared to a process where the parameters are mostly flat during all process production [71], [72].

Different approaches are possible for AM technologies where a model and adaptive strategy are not reliable yet. Most of them are based on the DOE strategy.

In the literature, it is possible to find a lot of work on process parameter optimization. The possible input parameters to optimize are multiple, and the output analysis could also change [28-38].

The parameters chosen are laser power, laser scanning speed, and material feed rate. [29,30,32,33,35,39-42]. From the literature, these 3 have major effects on the part production, mechanical properties, clad dimension, porosity and microstructure.

Other parameters could be added if a further optimization and refinement of the aimed output are needed.

But, adding parameters creates a higher number of samples or tracks to be analyzed.

If the number of parameters is reasonably low, it is possible to change one parameter, taking the other as a fixed value. Using this procedure, the effect of a single parameter change is observed in detail, but any influence of the other parameters changes is not taken into consideration. To solve this problem, it is possible to take a higher number of parameters trial and analyze their influence with parameter reduction [73], [85]. In this case, different combinations are possible, but reducing the number of parameters allows us to have a clear view of output change.

About possible output to analyze, based on the final aim of the experiment, the most common are melt pool or clad analysis [28,39,40,41,42], microstructure [30,31,34,35,42] porosity [16,30], mechanical properties [29,35] thermal model validation [77] or specific for some part production. [32,33].

## **Chapter 2.**

### **Materials and Methods**

The steps of the sample analysis could be divided as follows:

- Single Track Analysis → 48 Single Scan Tracks (SSTs)
- Single layer Analysis → 6 Single Layers (SLs)
- Single Wall Analysis → 12 Single Walls (SWs)
- 6 cubes

As main input variables, process parameters that have been analysed are the following:

Single track Analysis

- Laser Power [W]
- Laser Scanning Speed [mm/min]
- RPM of feed material
- Laser Focus [mm]

Single Layer Analysis

- Hatching Distance

Single Wall Analysis

- Overlapping (Z-step parameter)

For each step, other parameters are considered constant. At the end of the step, one or more combinations are chosen and used in the next step as new fixed parameters.

With the best combination of the first sets of process parameters, the final 6 cubes have been realized, and the following characteristics have been analysed:

- Superficial Porosity through Polishing
- Internal Porosity and Defects through Tomography
- Microstructure through Chemical Etching
- Hardness

## 2.1 DED Machine

The Ti6242 powder used in this thesis is a gas atomized spherical powder supplied by TLS GmbH, of Ti6242. The powder has a maximum of 50% of the reused powder.

All samples for analysis have been produced and supplied by IRIS srl. The samples have been produced with Borealis Cell, 6×4×1,5 m<sup>3</sup> chamber with an internal DED printing machine. The 3D head printer is placed on three Cartesian axes, traveling along X direction (4m long), in Y direction (1m) and Z direction (1m). In this case, the laser head and the deposition powder head are not on the same axis. The main components of the machine could be described as follows:

- The laser head, the terminal part, where the laser gets out directly onto the powder. The laser beam starts from the laser beam emission source, with an optical fiber system and is directed through an optical lens system to the laser head. To prevent metal powder pollution a final screening lens is located at the last end of the head. This latter is easily replaceable, while in case of fiber damage, the whole head should be replaced with a considerable stop of production.
- A laser Beam Emission Source can generate a laser with a power up to 3 kW.
- Chillers to reduce temperature with heat exchange through a solution of water and glycol. The main components on which chillers act are the optical laser system and the “Clamir” camera.
- Powder Feeder is made up of a rotating disk, with an inert gas inside. The change in the disk rpm, increases the powder flow to the nozzle.
- Computer
- Deposition head, located under the laser head, in this case the heads are not coaxial. Is made of a copper alloy, connected with the powder feeder through thin polymer tubes. The head is made of multiple nozzles to enhance the possibility of multi-material and guarantee a continuative power flow rate. The focus could be change through adjustment screws, but it should coincide with laser focus.
- Deposition tank, to collect all parts of unfused metal powder during the building process.
- Shielding gas head, to create the gas shield, avoiding reactive material get in contact with air oxygen. It's easily removable, for alloys for which is not required.
- Gas distribution system, outside of the Borealis cell, used to stock gas under pressure.
- “Clamir”, a thermal imaging camera. It's placed coaxial to the heads, it's used for monitoring the melting pool, implementing adaptive strategy and monitoring if some problems occur during building.
- Mobile Vacuum Cleaner, during printing process, a certain amount of unused powder is deposited inside the working area. The mobile vacuum cleaner is used to collect it. This amount of powder is then transferred into specific container, and then could be used again, mixed in a certain new powder
- Fixed Aspirator, on top of the cell, is needed to remove inert gases, combustion pollution and fine size powder particles.
- Control joystick for manual movement
- Roto-tilting table

- Air Compressor System, compressed air is used to feed movement of the axles and brakes of moving elements.

## 2.2 Cutting

The plates used to print up the parts are a  $110 \times 110 \times 8,5 \text{ mm}^3$  made of Ti64, with 4 holes for fixing it to the table.

To perform the cross-section analysis reported in the next chapter, the plate was cut into smaller samples, and the smaller samples were prepared with grinding and polishing.

The first cutting operation was performed in Polito through a Mekton Servocut 402-AA cutting machine as in “*Figure 2.1*”.



Figure 2.1: Mekton Servocut 402-AA

As a possible alternative, wire EDM was also taken into consideration to have a smoother and linear cut. However, because of its low machinability, the titanium alloy was not suitable for wire edm cut, since it would generate high wear on the wire.

In “*Error! Reference source not found.Figure 2.2*”, a schematic representation of the cut is ordered by the number of executions. Highlighted in green are the 6 samples for each plate that has then been used for microscope analysis

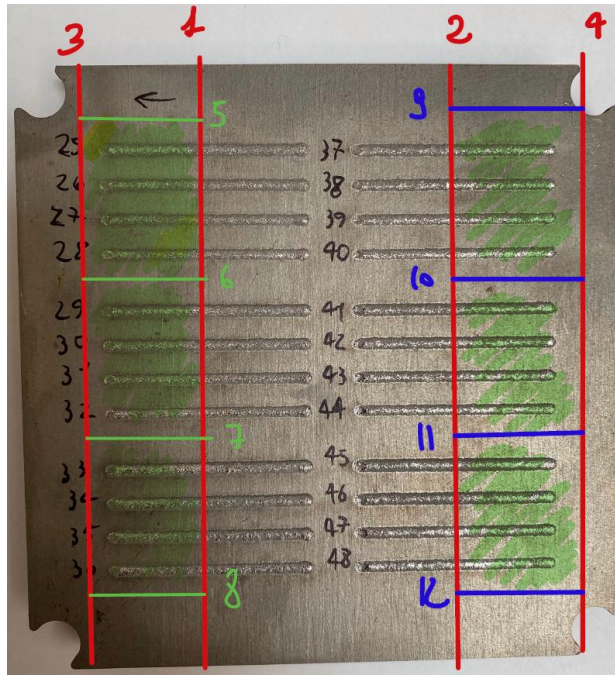


Figure 2.2: Cutting Pattern of Plates

## 2.3 Mounting

After cutting them all, the samples were mounted with acrylic resin. The resin used was a PRESI, KM-U, “Figure 2.3”, which is composed of two parts, powder and liquid.



Figure 2.3: Presi KM-U mounting resing

Mixing them together, with a ratio of 2:1, in about 15 minutes with heat realising, it becomes solid.

The mounting process has been executed manually using polyethylene molds. Due to too wide a sample, the automatic mounting machine was not able to be used. As an example, the result is shown in “Figure 2.4”.



Figure 2.4: Mounted samples

## 2.4 Grinding and Polishing

After the mounting process, the samples were polished. The polishing process was performed with a MINITECH 250 SP1, by PRESI “*Figure 2.6*”. It’s a manual polishing machine with the following specifications:

- Plate Diameter: 250 mm
- Rotation Speed: 20 to 700 RPM with 1rpm increment
- 750 W of nominal power
- Bidirectional rotation
- Watering by multijet ramp.



Figure 2.6: MINITECH 250 SP1 and sand paper disk

The polishing process itself was carried out multiple times due to the poor polishing properties of Titanium.

Multiple steps of sandpaper and a final diamond polishing suspension were used.

Between two subsequent steps, the direction of the sample has been rotated by 90 degrees. This allows to recognize if all the scratches from previous sandpaper have been completely removed.

The polishing cycle for each sample could be resumed as follows:

- Sandpaper 320 – 1 minute or more until complete removal of resin from the polished surface
- Sandpaper 600 – 5 minutes + scratch check. If needed, an additional 5 minutes.
- Sandpaper 800 – 5 minutes + scratch check. If needed, an additional 5 minutes.
- Sandpaper 1200 – 10 minutes + scratch check. If needed, an additional 5 minutes.
- Sandpaper 2400 - 10 minutes + scratch check. If needed, an additional 5 minutes.
- Sandpaper 4000 - 10 minutes + scratch check. If needed, an additional 5 minutes.
- Diamond Suspension Gel2+ polycrystalline 6 $\mu$  (by PRESI) on polishing cloths, Reflex PAD-MAG, HS-B – 30 minutes + polishing check. If needed, an additional 15 minutes.
- Diamond Suspension GEL2+ polycrystalline 3 $\mu$  (by PRESI) on polishing cloths, Reflex PAD-MAG, HS-B - 30 minutes + polishing check. If needed, an additional 15 minutes
- Diamond Suspension GEL2+ polycrystalline 1 $\mu$  (by PRESI) on polishing cloths, Reflex PAD-MAG, NT - 30 minutes + polishing check. If needed, an additional 15 minutes

The expected result was a mirror surface, without multiple scratches. If multiple scratch appeared during the process, based on the depth of the scratch, the sandpaper process has been rerun, with a direction perpendicular to the scratch, until their disappearance. The samples, were then cleaned with water, and dried with a heat source to remove water halos.

## 2.5 Stereo Microscope and Optical Microscope

For the analysis the following material has been used:

- Stereo microscope MZ10F by Leica, “Figure 2.7”

-



Figure 2.7: Stereo microscope MZ10F by Leica

- Optical Microscope DM6 by Leica, “Figure 2.8”.



Figure 2.8: Optical Microscope DM6 by Leica

## 2.6 Chemical Hatching Process

After the polishing process, to highlight the mechanical structure of the final samples, a chemical etching was performed using Kroll's reagent (100ml H<sub>2</sub>O, 1-3 ml hydrofluoric acid 65%, and 2-6 mL nitric acid).

The samples were submerged in the solution for 8 seconds, immediately rinsed in distilled water, dried with hot air, and analysed with an optical microscope.

## 2.7 Tomography

With tomography it is possible to construct a 3D model of a real part, using X-ray. The X-ray in a rotating table hits the part and is finally captured by a detector. With an internal algorithm, the X-rays detected are used to build a 3D model of the parts, which shows porosity. The porosity in this case could be compared to the one seen in the cross-section analysis of the sample. Furthermore, a larger overview of the porosity could be analyzed with respect to the section analyzed, and additional data on porosity distribution, geometry, and diameter of the pores is also available with this technology.

For this purpose, a Phoenix v|tome|x s 240 has been used as “*Figure 2.9*”.



Figure 2.9: Tomograph by Phoenix

## 2.8 Hardness

For measure the hardness of the final part, a Wilson VH1150 has been used, as “*Figure 2.10*”. The tester has a Vickers diamond indenter and has the hardness on the crosscut section of the final samples.



Figure 2.10: Microhardness tester Wilson VH1150

## **Chapter 3.**

### **Results And Discussion**

#### **3.1 Single Track Analysis**

As the first step of the thesis, a single-track analysis was performed. In this part, the main focus is the definition of a suitable combination of power, laser speed, powder flow rate, and laser focus, to proceed with the next steps.

As a main output, the width and height of the track were analyzed, after grinding and polishing the track, using an optical microscope.

##### **3.1.1 Parameters Overview**

As a starting point, a similar known printable alloy has been taken into consideration. Ti64 has been individuated as the most suitable due to its similarity to Ti6242 and is widely used in production.

The Ti64 starting parameters were taken from the IRIS srl alloy database based on previous parameter optimization and company know-how.

From Ti64 data, the main parameters have been modified in a range of 3 values for laser power, 4 values for speed, 2 values for laser focus, and 2 values of rpm, creating 48 possible combinations of parameter for tracks. (Table 3.1 and Table 3.2)

All tracks have been numbered with a growing numerical index starting from 1 up to 48.

Tracks have been divided into 2 plates for spacing reason. (*“Figure 3.1”* and *“Figure 3.2”*)

Here is a table resuming all the track numbers with related main parameters.

All other minor parameters have been considered the same for all other tracks, such as the shielding gas, the shielding gas flow rate, the room temperature, etc.

The plate is a 110×110×8,5mm<sup>3</sup> made of Ti64, with 4 holes for fixing it to the table.

Table 3.1 – First Plate Tracks parameter summary

Plate 1					
# Track	Laser Power (W)	Speed (mm/min)	Laser Focus (mm)	Powder Flow Rate (g/min)	Powder Flow Rate (rpm)
1	750	600	6,5	6,77	4
2		700			
3		800			
4		900			
5	850	600			
6		700			
7		800			
8		900			
9	950	600			
10		700			
11		800			
12		900			
13	750	600	8,5		
14		700			
15		800			
16		900			
17	850	600			
18		700			
19		800			
20		900			
21	950	600			
22		700			
23		800			
24		900			

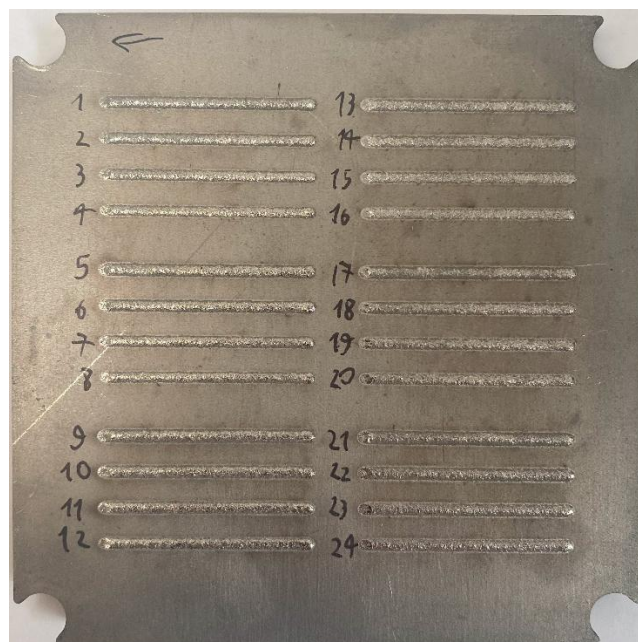


Figure 3.1: First Plate Track Parameter

Table 3.2 – First Plate Tracks parameter summary

Plate 2					
# Track	Laser Power (W)	Speed (mm/min)	Laser Focus (mm)	Powder Flow Rate (g/min)	Powder Flow Rate (rpm)
25	750	600	6,5	10,25	6
26		700			
27		800			
28		900			
29	850	600			
30		700			
31		800			
32		900			
33	950	600			
34		700			
35		800			
36		900			
37	750	600	8,5		
38		700			
39		800			
40		900			
41	850	600			
42		700			
43		800			
44		900			
45	950	600			
46		700			
47		800			
48		900			

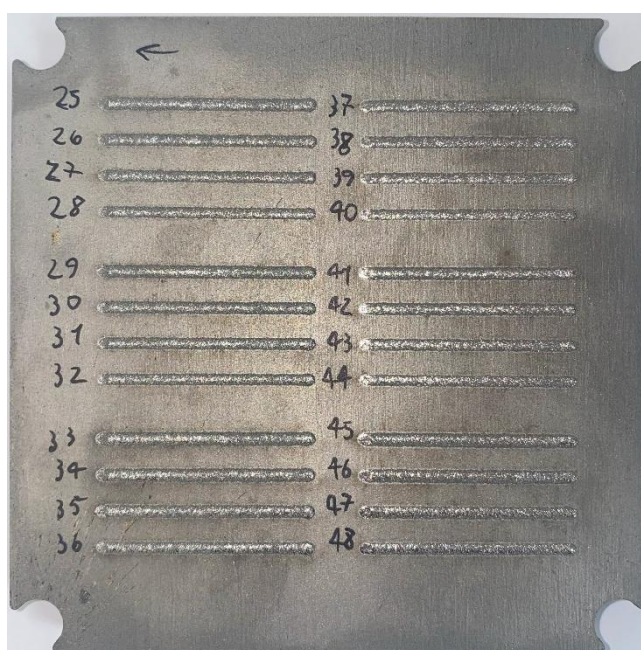


Figure 3.2: First Plate Track Parameter

### 3.1.2 Microscope Analysis

The parts have been prepared according to “**Error! Reference source not found. Error! Reference source not found.**”.

- **Top view analysis**

Two different Microscopes were used.

First, a modular stereo microscope MZ10F by Leica was used, and the first inspection of the overall tracks was conducted. The tracks have been analysed from the top view with different microscope resolution  $1\times$  and  $3\times$ . Also, a general view at  $5\times$  has been given, but the photo result as not significant due to too high magnification.

As it's possible to see from “*Figure 3.4*” to “*Figure 3.11*”, all the tracks have been successfully deposited. It is also possible to notice the direction of deposition as shown in “*Figure 3.3*”, at the starting deposition point on the left and at the end deposition point on the right.

With a first view, analysing the size of the SST with respect to unmelted powder, the increase in power leads to a larger melt powder, while the increase in speed reduces it. The focus has a major role in the spread of the hit zone of melting. The lower the focus, the thinner the melted part, with a major focus on the centre of the tracks. Finally, the powder flow rate is the balance factor that creates a good ratio between melted and unmelted tracks.

From this first analysis, it is possible to appreciate that, as in “*Figure 3.5*” and in “*Figure 3.7*”, for all the combination of power and scan speed, the tracks result as strongly heterogeneous. In “*Figure 3.7*”, the whole track is almost fully melted, while in “*Figure 3.5*” the central part of the track is fully melted without any powder remaining. This difference is caused by difference in focus, with the higher focus spreading the power over all the melting tracks. This behaviour could be possible both by too high power or too low powder flow rate. Indeed, in “*Figure 3.9*” and “*Figure 3.11*”, due to the higher amount of powder, the tracks result more homogeneous, even if for higher power, the central zone is still fully melted, in particular for low scan speed (i.e. track 33, 36 in “*Figure 3.9*” and 45, 48 in “*Figure 3.11*”). Despite these first observations, a cross-section analysis is needed to fully understand the track deposition. Only with the whole overview of the data is possible to choose the most suitable parameters to adopt in the next steps.

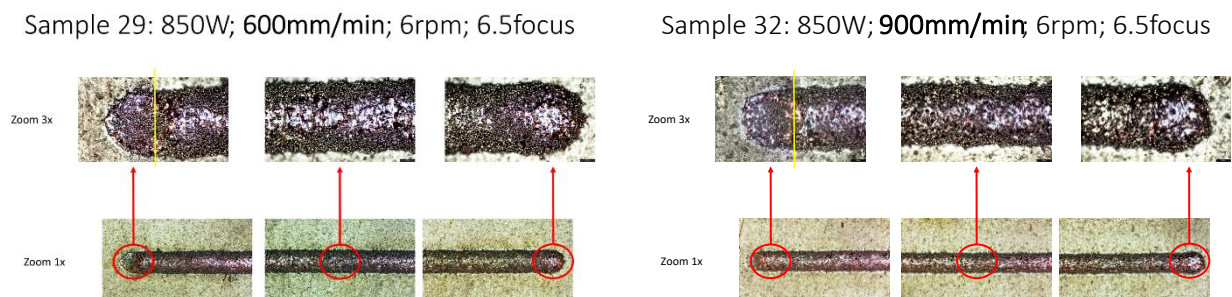


Figure 3.3: Example of tracks with a focus on their extremities

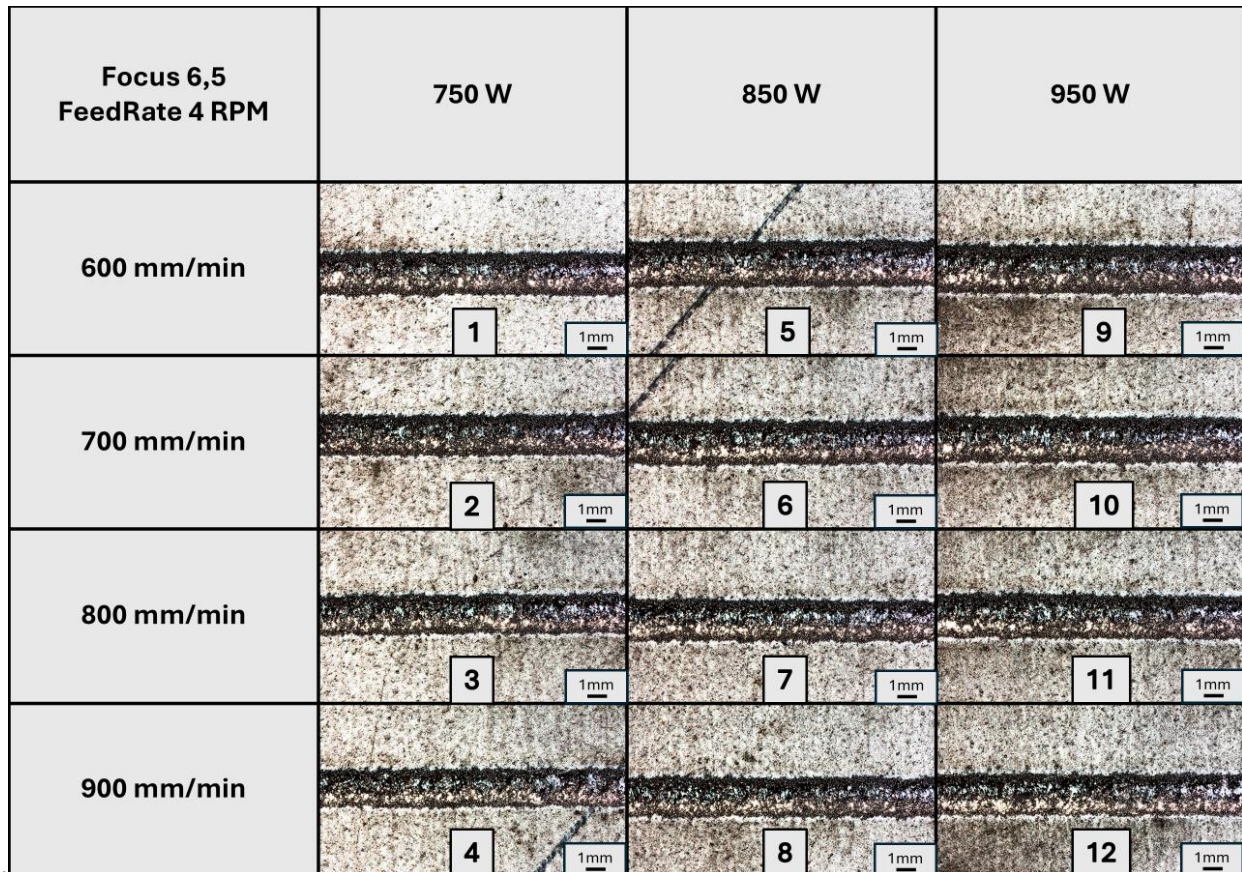


Figure 3.4: Tracks 1 to 12, 1× resolution

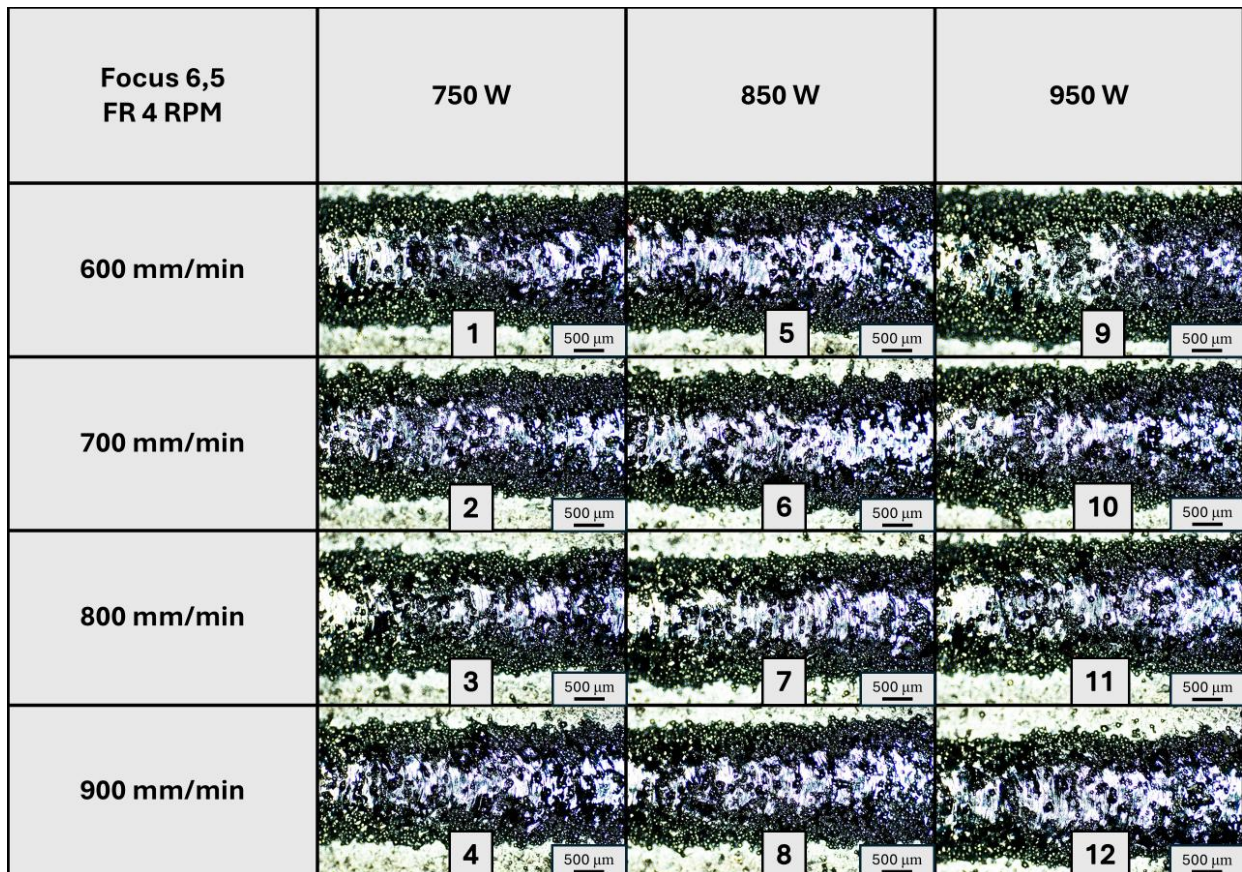


Figure 3.5: Tracks 1 to 12, 3× resolution

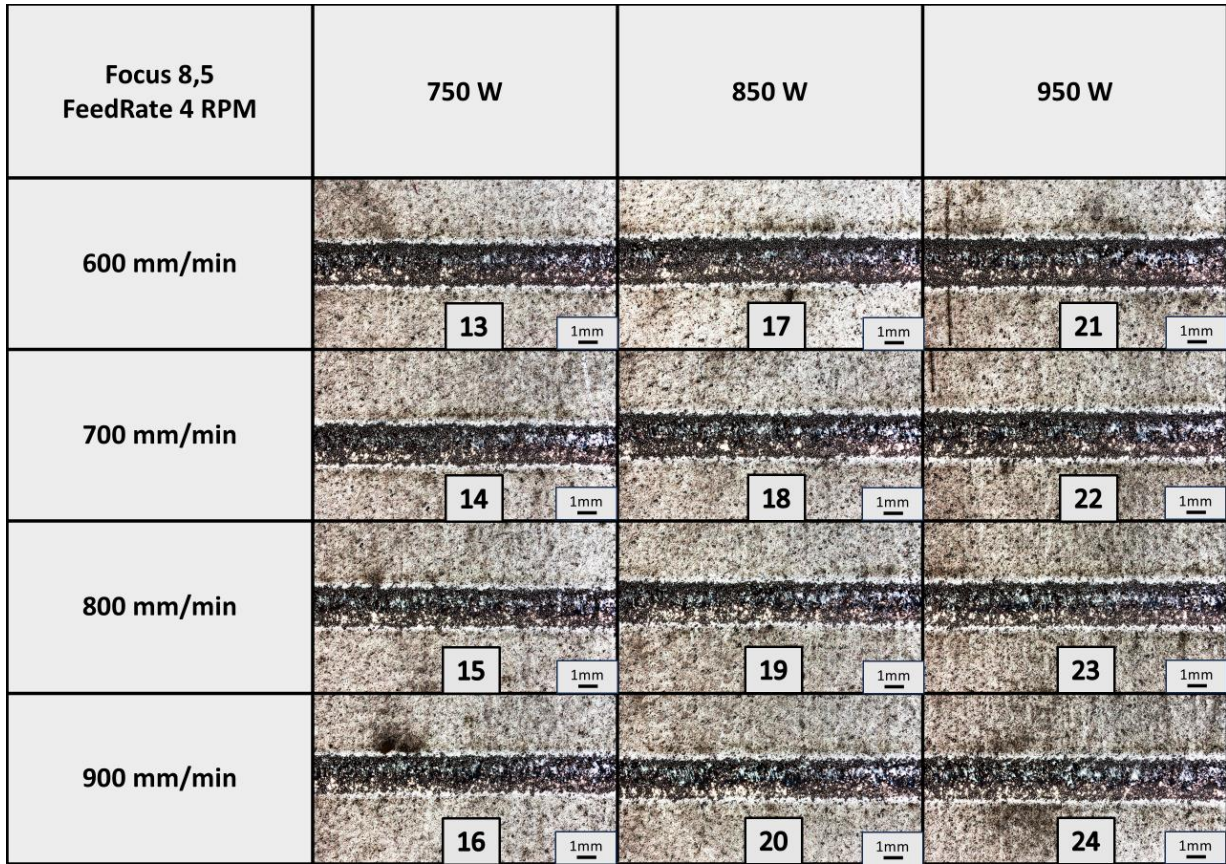


Figure 3.6: Tracks 13 to 24, 1× resolution

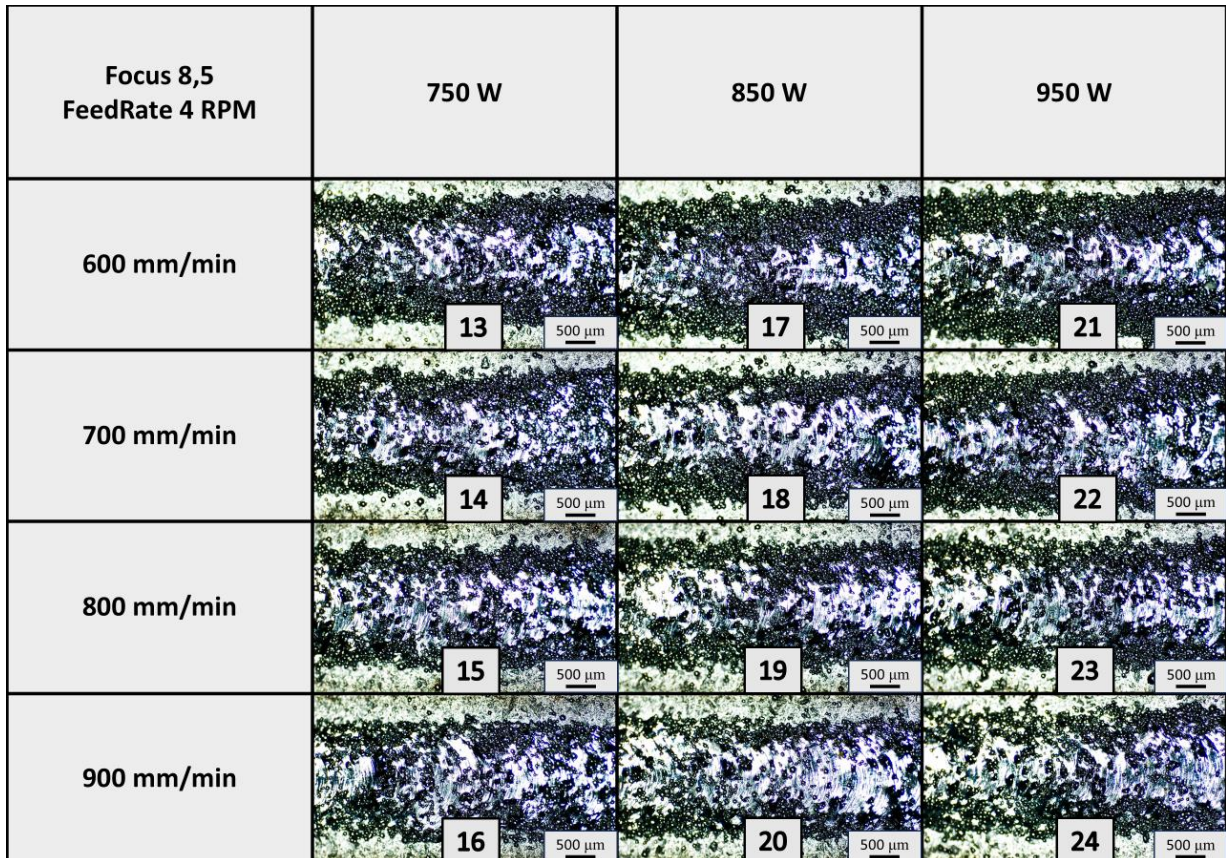


Figure 3.7: Tracks 13 to 24, 3× resolution



Figure 3.8: Tracks 25 to 36, 1× resolution

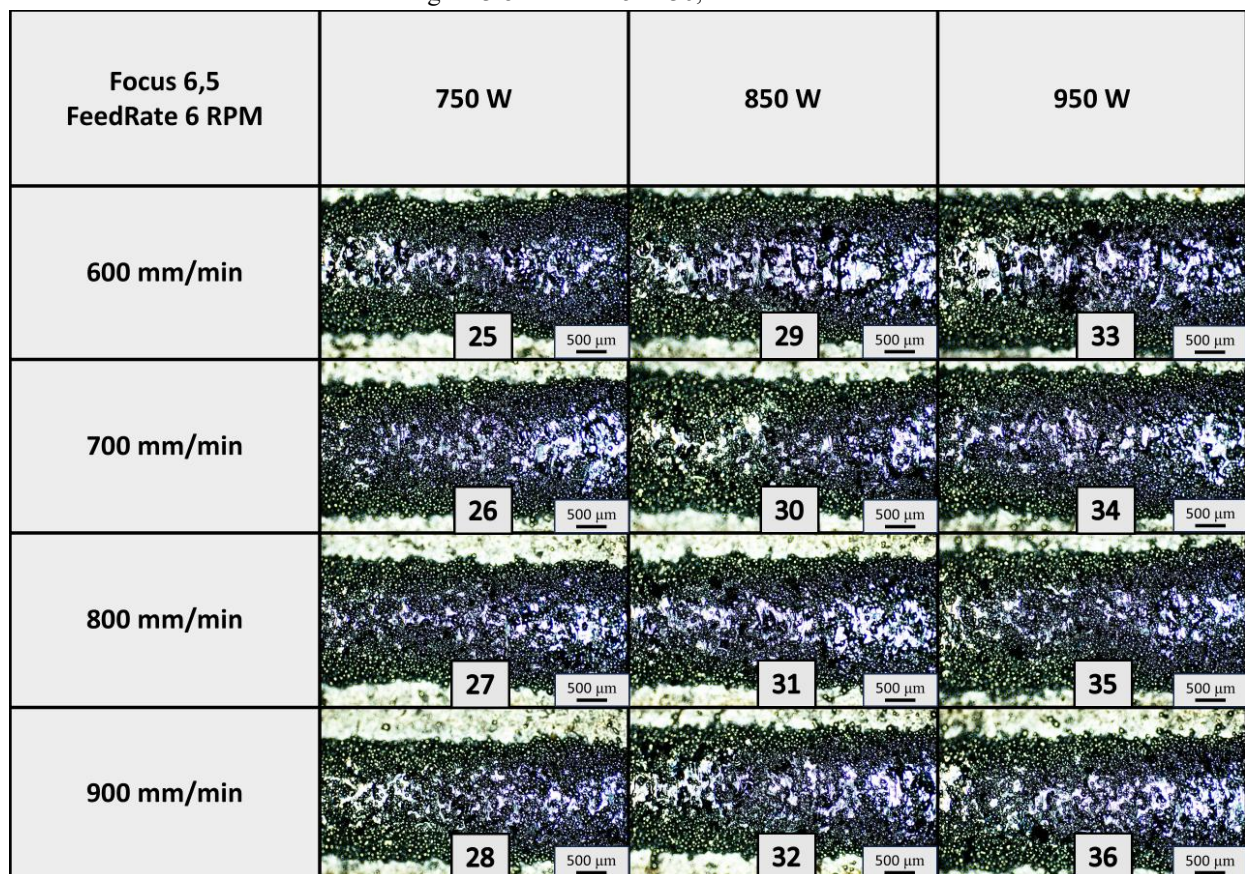


Figure 3.9: Tracks 25 to 36, 3× resolution

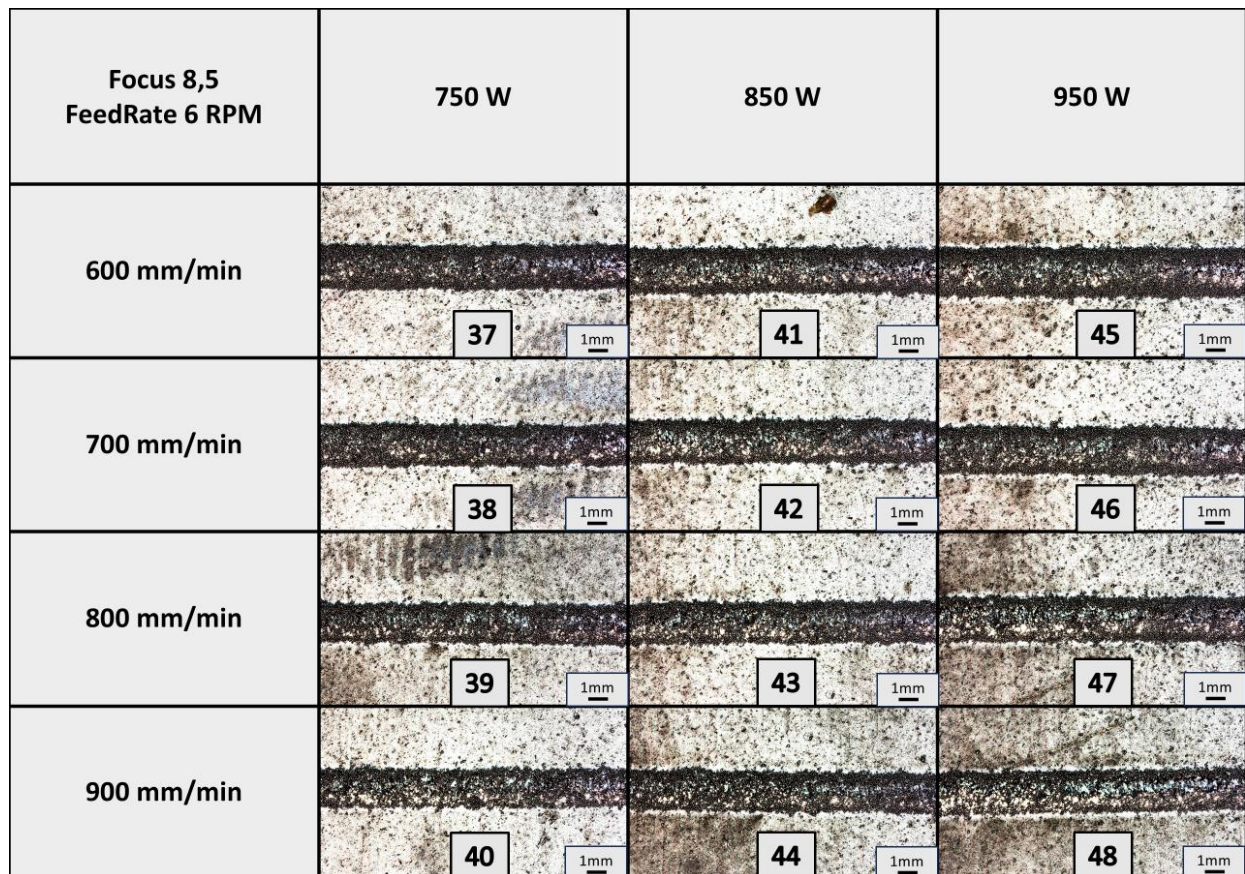


Figure 3.10: Tracks 37 to 48, 1× resolution

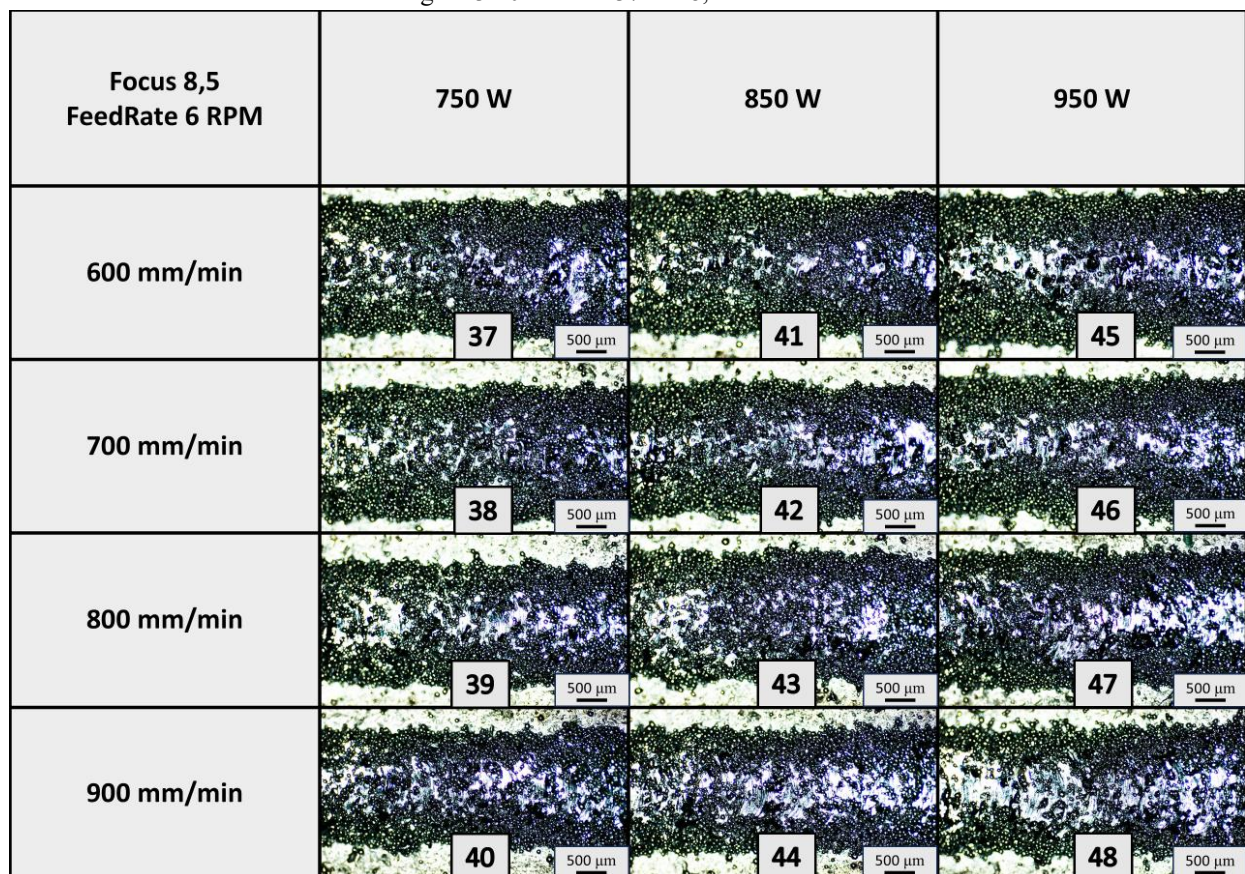


Figure 3.11: Tracks 37 to 48, 3× resolution

- **Cross section analysis**

In “Figure 3.16” to “Figure 3.19”, all the cross-sections are reported. With ImageJ, the 2 main dimensions were measured and reported in “Table 3.3”.

Table 3.3: Tracks dimensions report

# Track	Width [mm]	Height [mm]	# Track	Width [mm]	Height [mm]
1	1821	491	25	1883	645
2	1696	432	26	1899	587
3	1848	365	27	1916	465
4	1640	271	28	1705	441
5	2030	484	29	2018	747
6	1949	432	30	1913	609
7	1729	348	31	1816	562
8	1733	390	32	1781	502
9	2205	552	33	2247	769
10	2043	428	34	2005	613
11	1912	397	35	2074	536
12	1886	325	36	1845	516
13	1884	277	37	2099	367
14	1970	221	38	1993	315
15	1761	177	39	1736	259
16	1782	186	40	1670	276
17	2068	284	41	1926	418
18	1957	212	42	1894	345
19	1878	191	43	1932	313
20	1794	183	44	1750	253
21	2194	286	45	2089	404
22	1996	221	46	2049	347
23	2052	225	47	2143	320
24	2041	169	48	1958	286

Data was reported and graphed to see the effects of the variable parameters, as shown in “Figure 3.12” & “Figure 3.13”. Analyzing the dimensions change is possible to state the following:

- Increasing speed decreases both dimensions but significantly extends height more than width. As shown in “Figure 3.13”, on the lower part of the graph, all the height trend lines are lowering as the scan speed increases (x axis).

On the width, instead, the effect of speed on dimension change is not clear. Passing from 600 to 900 mm/s, the general trend is a decrease in section dimension, but at the intermediate velocity it really depends on the other parameters.

For high power (“Figure 3.12.c”) having a higher focus or higher material rate, smooth the descending trend of the width.

For medium power, the general trend of the width diminishes with low scan speed. The single increase in the line representing focus 8,5 and 6 feed rate (“Figure 3.12.b”) is a

single point out of trend. So, it's realistic to suppose it as an outlier, with possible error during manufacturing or measuring processes.

For low power, ("*Figure 3.12.a*"), the overall speed effect from 600 to 900 mm/s is to decrease the width. However, the behaviour for intermediate speed is not so clear. From 700 to 800 mm/s is possible to see that having a Focus at 8,5 make the width decrease, while with focus at 6,5 the behaviour is the opposite.

- Focus and feed rate have a major effect on the height rather than width. It is possible to see that, even if the trend of the width lines ("*Figure 3.12*") is not linear, they are near between them, so the change in parameter does not affect the width so much. Instead, the height lines ("*Figure 3.13*") are more separate, meaning a higher impact of these two parameters on height change, as shown in "*Figure 3.12*" and "*Figure 3.13*".
- For any power and any speed, the Feed Rate increase led to a higher height, as shown in "*Figure 3.13*", comparing yellow lines with brown lines (F8,5FR4 -> F8,5FR6) and orange lines with green ones (F6,5FR4 -> F6,5FR6).
- For any power and any speed, focus increase led to a lower height as shown in "*Figure 3.13*", comparing orange lines with yellow lines (F6,5FR4 -> F8,5FR4) and green lines with brown ones (F6,5FR6 -> F8,5FR6).
- From the previous points, it is also possible to compare the effect of focus and the effect of feed rate on height change. It is possible to state that a decrease in focus has a major impact with respect to an increase in feed rate. As shown in *Figure 3.13*, taking into attention the yellow lines, the height becomes higher, decreasing the focus (orange lines) rather than increasing the feed rate (brown lines).
- From "*Figure 3.14*" and "*Figure 3.15*", it is also possible to have a clear view of the change in power for different velocities. As shown in "*Figure 3.14*", the effect of increased power is to increase the width, even if at medium velocity the change in power is smoothed. Furthermore, at low velocity, with an 8.5 feed rate and 6 focus, the change in power is not so relevant with respect to the other parameter configuration ("*Figure 3.14a-b*" orange line). On the other hand, as in "*Figure 3.15*", power does not significantly impact height.

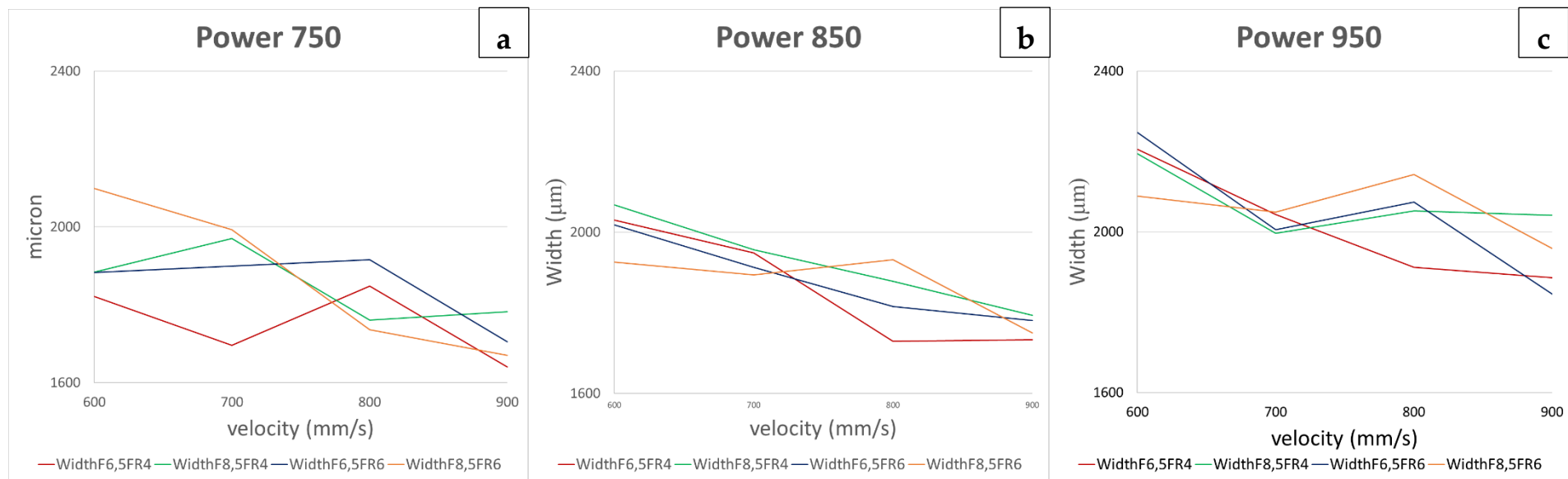


Figure 3.12: Effect on width for different Power

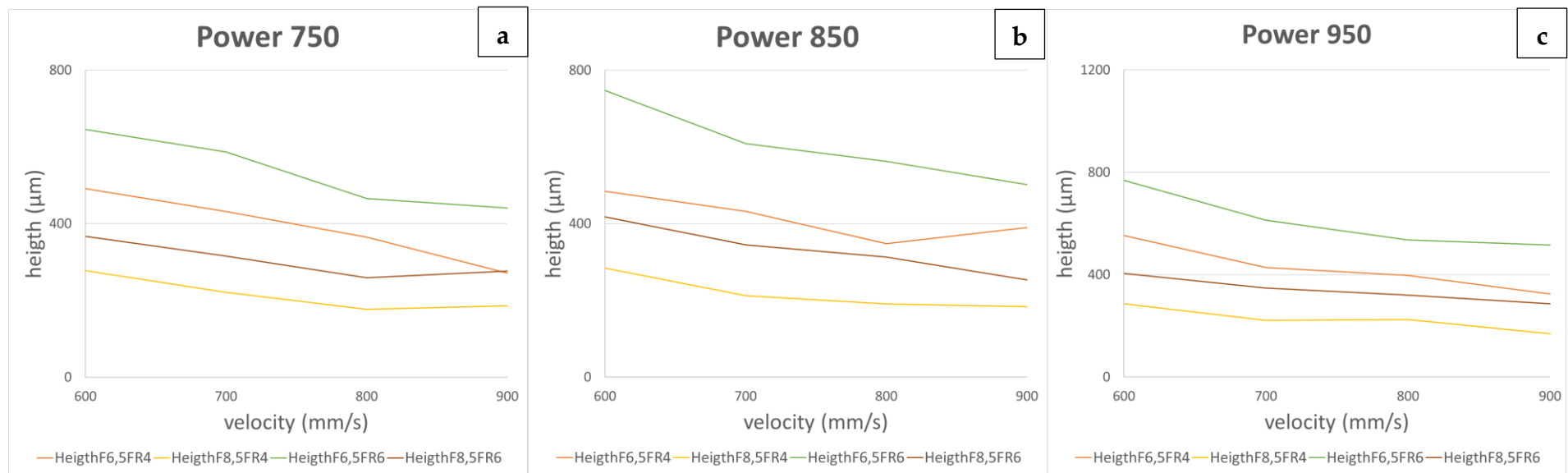


Figure 3.13: Effect on height for different Power

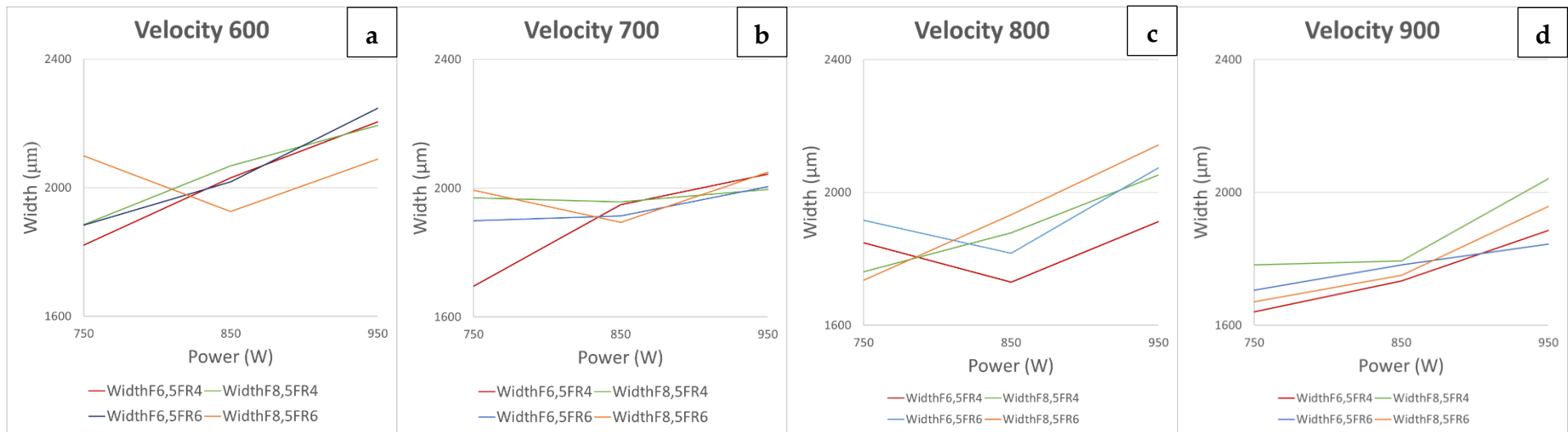


Figure 3.14: Effect on width for different velocity

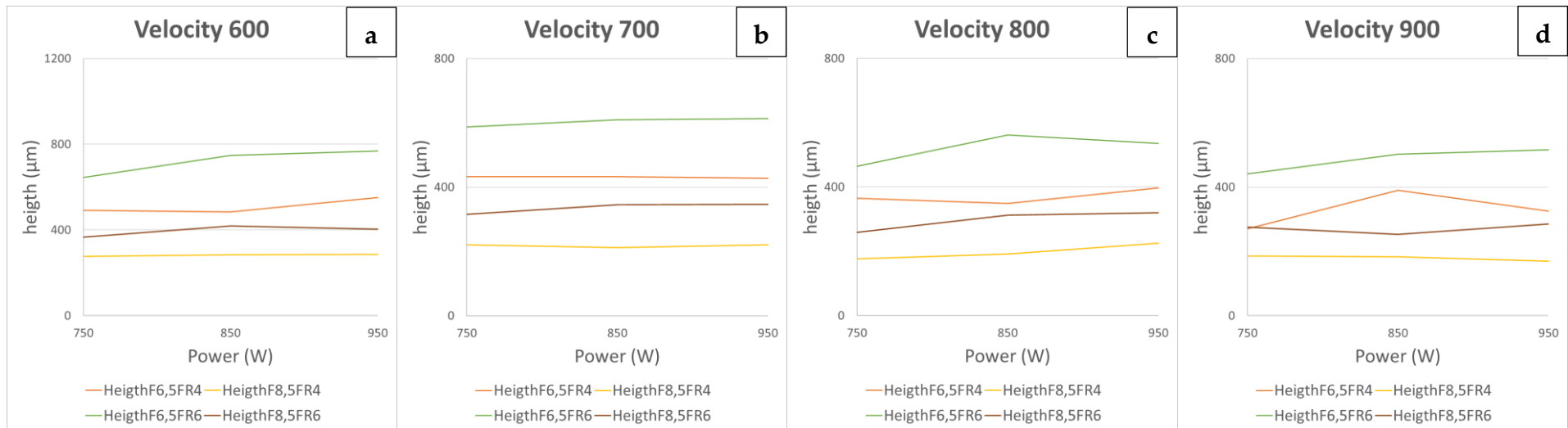


Figure 3.15: Effect on heigth for different velocity

Getting in deeper detail on the section of the analysed tracks, the focus is the shape of the tracks themselves. A good parameter for analyzing the shape is the width-to-height ratio. Here in Table 3.4, all ratios are reported:

Table 3.4: Ratio of Tracks

# Track	Width [mm]	Height [mm]	Ratio W/H	# Track	Width [mm]	Height [mm]	Ratio W/H
1	1821	491	3.709	25	1883	645	2.919
2	1696	432	3.926	26	1899	587	3.235
3	1848	365	5.063	27	1916	465	4.120
4	1640	271	6.052	28	1705	441	3.866
5	2030	484	4.194	29	2018	747	2.701
6	1949	432	4.512	30	1913	609	3.141
7	1729	348	4.968	31	1816	562	3.231
8	1733	390	4.444	32	1781	502	3.548
9	2205	552	3.995	33	2247	769	2.922
10	2043	428	4.773	34	2005	613	3.271
11	1912	397	4.816	35	2074	536	3.869
12	1886	325	5.803	36	1845	516	3.576
13	1884	277	6.801	37	2099	367	5.719
14	1970	221	8.914	38	1993	315	6.327
15	1761	177	9.949	39	1736	259	6.703
16	1782	186	9.581	40	1670	276	6.051
17	2068	284	7.282	41	1926	418	4.608
18	1957	212	9.231	42	1894	345	5.490
19	1878	191	9.832	43	1932	313	6.173
20	1794	183	9.803	44	1750	253	6.917
21	2194	286	7.671	45	2089	404	5.171
22	1996	221	9.032	46	2049	347	5.905
23	2052	225	9.120	47	2143	320	6.697
24	2041	169	12.077	48	1958	286	6.846

Taking into example “Figure 3.16” and “Figure 3.17”, the ratio is always high. Going into the section view, it is possible to observe that the tracks are very wide, and the hump of the track is not so evident. This is probably due to low powder on the sample or too high speed with respect to other parameters. This confirms what was observed in “Top view analysis” where the melted powder was visible throughout the track. A similar effect is present in “Figure 3.19”, even if to a lower extent. In this case the effect of flattening of the tracks is less evident with respect to “Figure 3.17”, because of the higher powder flow rate, but the focus at 8.5 generates a less shaped tracks with respect to “Figure 3.18”, which has the same powder flow rate but a focus of 6,5mm.

Based on the previous, the best-shaped tracks are obtained with parameters reported in “Figure 3.18”, namely 6,5mm focus, 6rpm feed rate.

Tracks 25 – 29 – 33 have the opposite behaviour of the previously described tracks. These 3 have a vertical dimension that is overdeveloped with respect to the width.

Tracks 28 – 32 – 35 have a poor interface between the base plate, and the contour of the track is not round.

Tracks 27 – 31 have a not well-rounded contour.

Among the remaining tracks, namely 26-30-34-36, all share a good shape and a good ratio w/h. However, track 36 was the flattest among the 4, while 34 showed little imperfection at the interface between the plate and the shape was the less rounded among the 4.

Parameters of tracks 26 and 30 have been chosen for the next steps resulting in the most well-shaped tracks deposited in this step. It is possible to appreciate that the ratio of the two tracks is very similar, around 3.2. Suppose this ratio could be considered the most suitable for a round-shaped track, in that case it is easier to see the resulting ratio is quite different for combination of parameter in “*Figure 3.16*”, “*Figure 3.17*” and “*Figure 3.19*”.

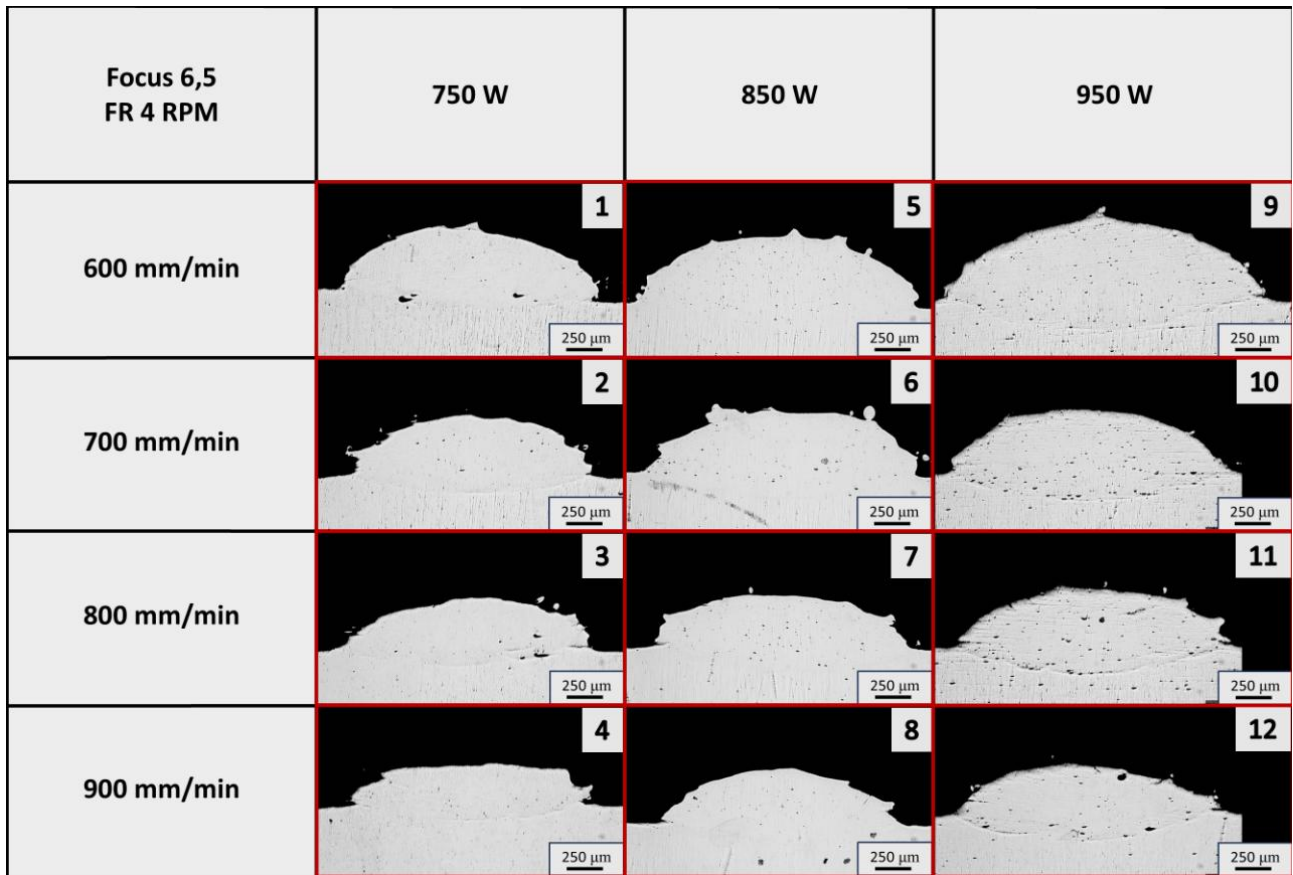


Figure 3.16: Cross section analysis tracks 1 to 12

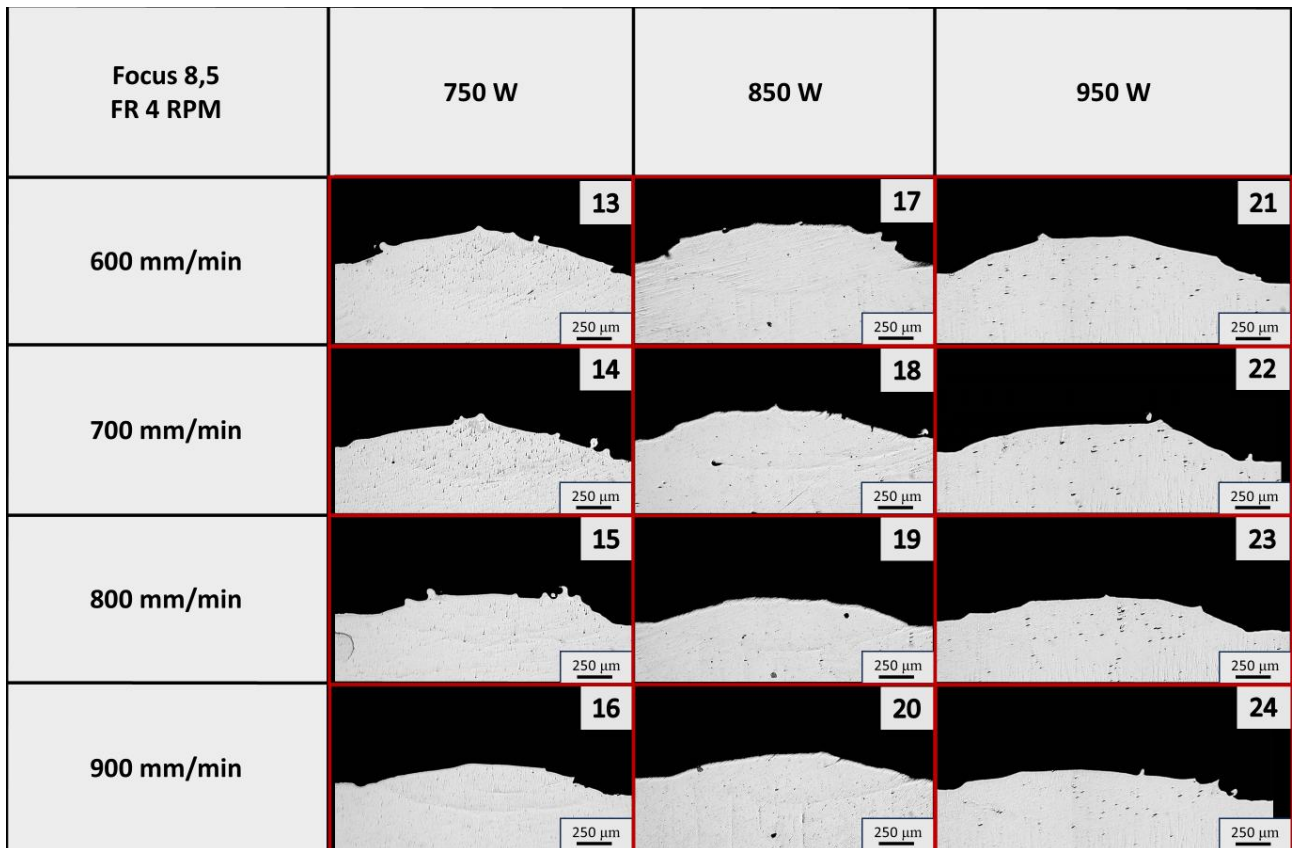


Figure 3.17: Cross section analysis tracks 12 to 24

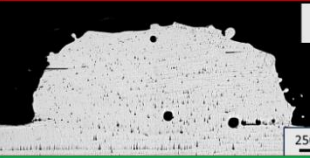
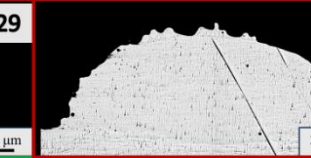
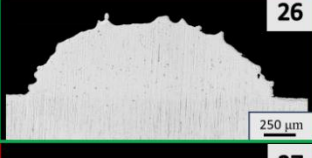
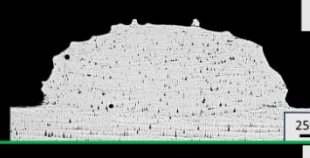
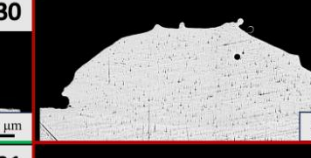
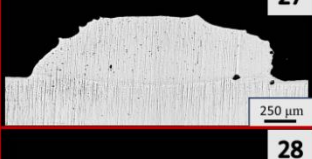
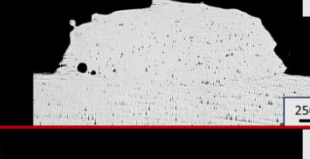
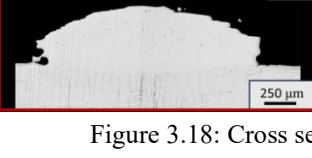
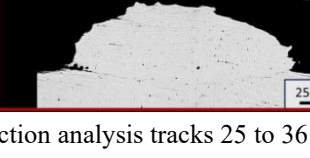
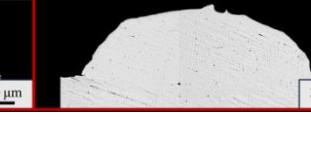
Focus 6,5 FR 6 RPM	750 W	850 W	950 W
600 mm/min	 25	 29	 33
700 mm/min	 26	 30	 34
800 mm/min	 27	 31	 35
900 mm/min	 28	 32	 36

Figure 3.18: Cross section analysis tracks 25 to 36

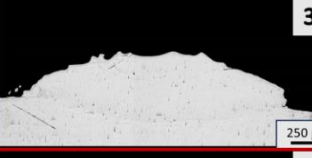
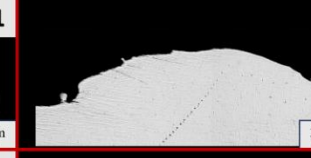
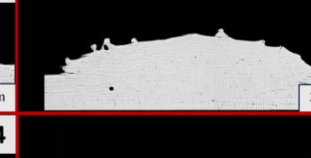
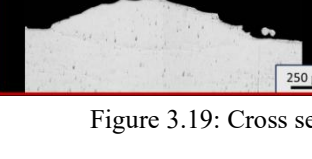
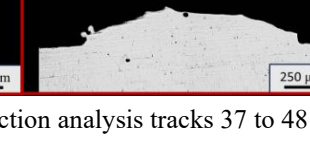
Focus 8,5 FR 6 RPM	750 W	850 W	950 W
600 mm/min	 37	 41	 45
700 mm/min	 38	 42	 46
800 mm/min	 39	 43	 47
900 mm/min	 40	 44	 48

Figure 3.19: Cross section analysis tracks 37 to 48

- **Parameters for Single Layer and Single Wall Analysis**

As for previous paragraphs, the two combinations of parameters chosen for the next steps are the following:

# Track	Laser Power (W)	Speed (mm/min)	Laser Focus (mm)	powder flow rate (g/min)	Width [mm]	Height [mm]	Ratio W/H
26	750	700	6,5	10.25	1899	587	3.235
30	850	700	6,5	10.25	1913	609	3.141

## 3.2 Single Layer Analysis

Once parameters from previous steps were chosen to pass from a single track to a final part printing, hatch distance, and height distance were analysed.

Hatching distance is the distance between 2 adjacent layers, and it's usually indicated as a percentage. For example, a 25% hatching distance for example means that 2 layers have been overlapped for a 25% of the track width.

### 3.2.1 Parameters Overview

In this case, 3 levels of hatching were analysed for both sets of parameters chosen from the previous step, for a total of 6 tracks. A recap of the main parameters is shown in Table 3.5.

Table 3.5: Single Layer Tracks Parameters

Plate 3					
# Track	Laser Power (W)	Speed (mm/min)	Laser Focus (mm)	Powder Flow Rate (rpm)	Hatching (%)
1	750	700	6.5	6	25
2	750	700	6.5	6	50
3	750	700	6.5	6	75
4	850	700	6.5	6	25
5	850	700	6.5	6	50
6	850	700	6.5	6	75

The plate “*Figure 3.20*” is a  $110 \times 110 \times 8.5 \text{mm}^3$  made of Ti64, with 4 holes for fixing it to the table, and has on it the 6 tracks of single walls analysis and the 12 tracks of “*3.3 Single Wall Analysis*”.

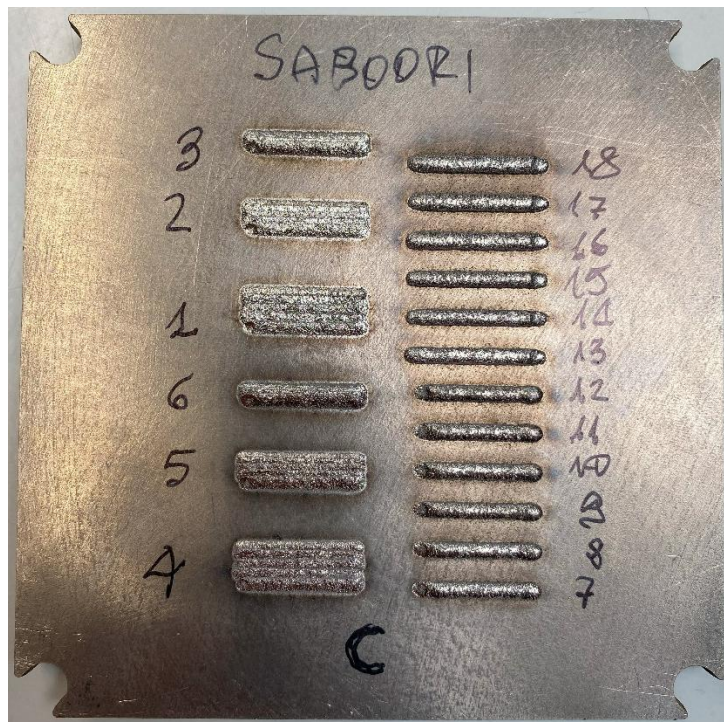


Figure 3.20: Plate with single layer analysis and single walls analysis

### 3.2.2 Microscope Analysis

The parts have been prepared according to “Error! Reference source not found. Error! Reference source not found.”.

- **Top view analysis**

In “Figure 3.21”, the top-view photos are reported. The photos are obtained with the stereo microscope at different resolutions (1× and 3×). All tracks have been successfully deposited.

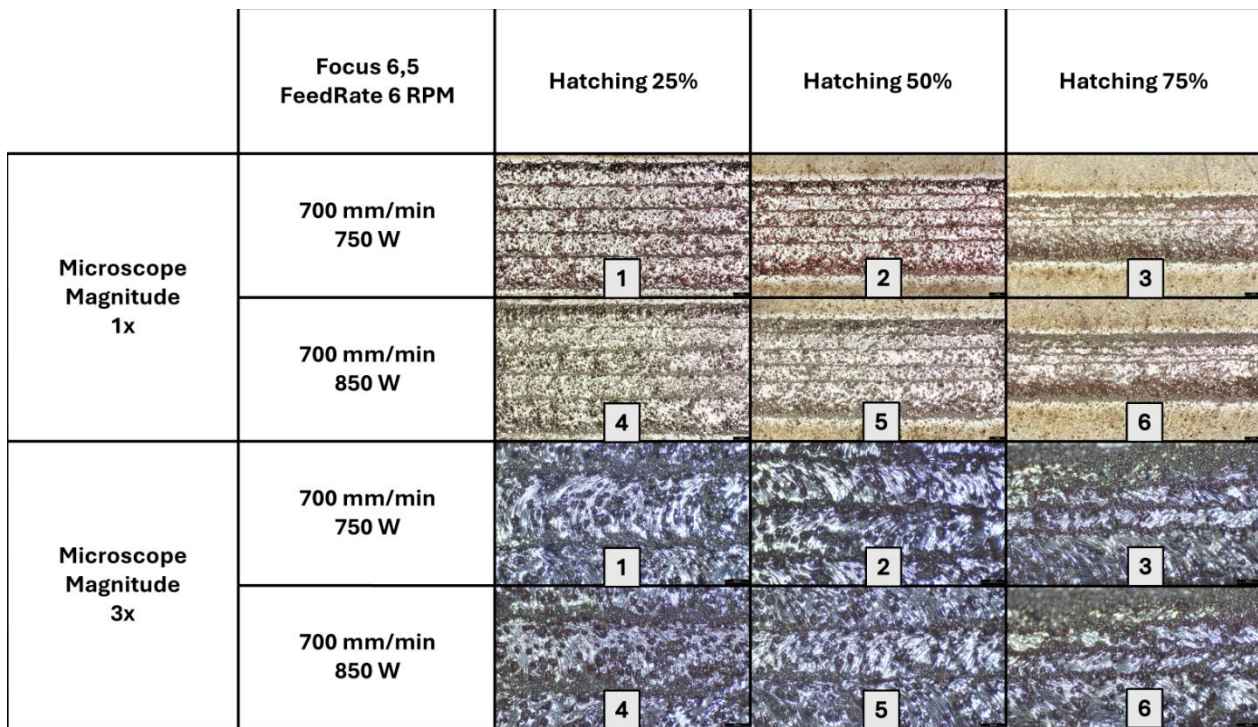


Figure 3.21: Top View of Tracks for Single Layer analysis

In “Figure 3.22”, the cross-sections of the 6 tracks are reported. For the single layer analysis, the focus is the shape of all layers joined.

In Table 3.6 the width and height of the tracks were measured and reported with ImageJ.

Table 3.6: Layer Track dimension

# Track	Width [mm]	Height [mm]	Ratio W/H
1	7749	364	20.61
2	5714	506	11.29
3	3831	812	4.72
4	7626	394	19.81
5	5651	502	11.26
6	3450	819	4.21

Starting from track 1 and 4, it is possible to notice the gap between one layer and the adjacent one. This means the tracks are still too far from each other, and the gap between the two subsequent layers could potentially cause porosity when the full part is created.

In tracks 3 and 6, instead, it is possible to notice that the right part of the circular shape deposition is not round and has discontinued form. The discontinuities are tight, and the central part of the deposition is very developed in height with respect to the lateral part of the pool, in fact the ratio width to height is very similar to the single track analysed in the previous chapter (around 3.2). These suggest that the overlapping of the layers is too high, with an over amount of material in the central part of the track.

Instead, tracks 2 and 5 show a quite round shape, with a good proportion of width/height.

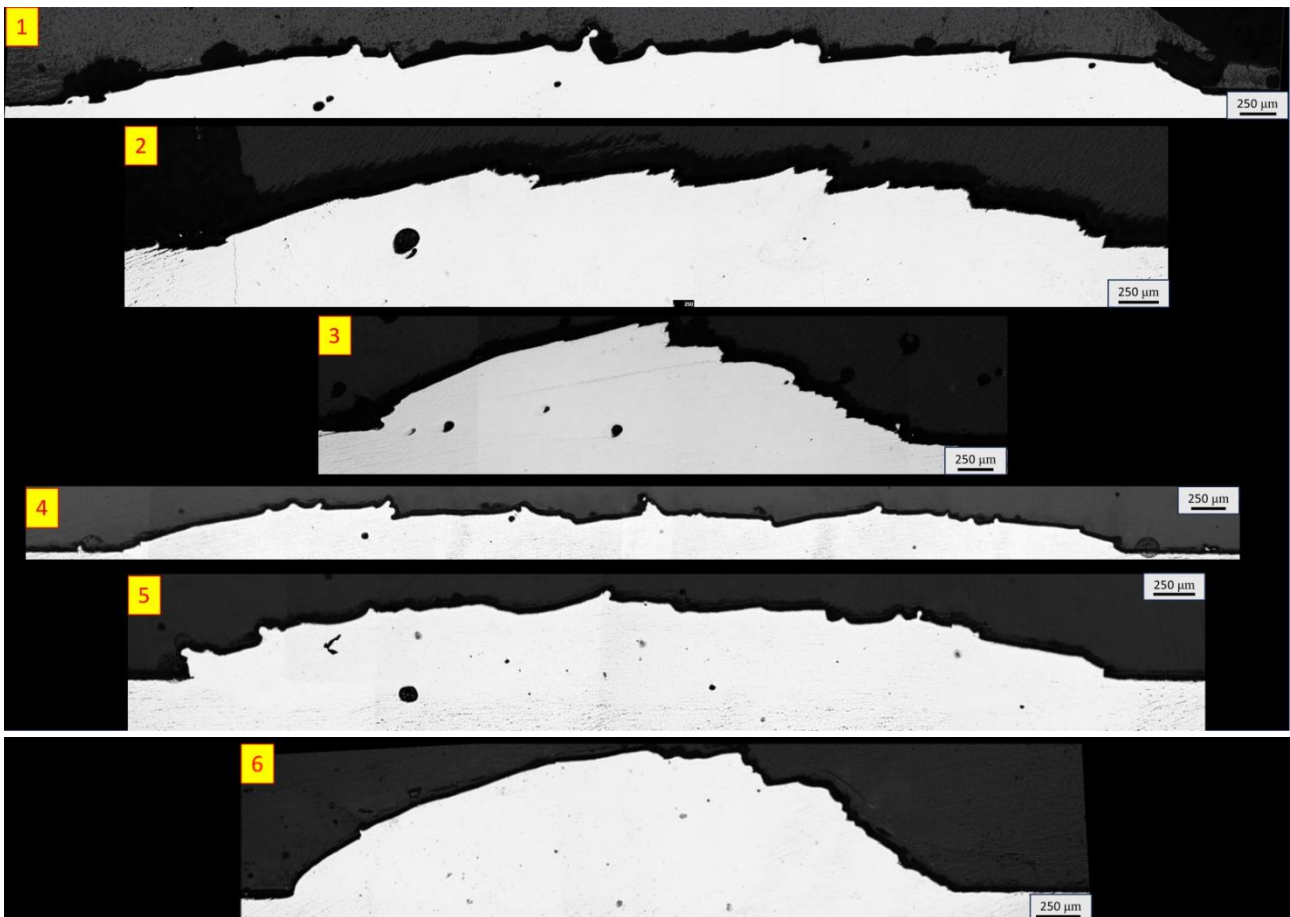


Figure 3.22: Cross-section analysis tracks 1 to 6 for Single Layer analysis

- **Parameters for Cube creation**

As for previous paragraphs, the two combinations of parameters chosen for the next steps are the following:

# Track	Laser Power (W)	Speed (mm/min)	Laser Focus (mm)	powder flow rate (g/min)	Hatching (%)	Pitch (mm)	Ratio W/H
2	750	700	6.5	10.25	50	0.9495	11.29
5	850	700	6.5	10.25	50	0.9565	11.26

### 3.3 Single Wall Analysis

The last main parameter to tune is the height distance between the 2 layers. Also, for this analysis, the distance between 2 overlaid layers was analyzed and 3 different parameters and 2 different strategy of deposition were chosen.

The Z-step distance between the 2 layers has been set to 25, 50, and 75%, while 2 different strategies of deposition have been used with monodirectional deposition or bidirectional deposition. The same number of layers have been deposited for each different step (5 layers).

As a clarification, 25% of Z-step means a vertical overlaying of 75% of two subsequent layers. So, a 25% Z-step will have, with the same amount of layers, lower height with respect to a 75% Z-step track.

#### 3.3.1 Parameters Overview

In this case, 3 levels of hatching have been analyzed for both sets of parameters chosen from the previous step, for a total amount of 6 tracks for each deposition strategy. A recap of the main parameters is shown in Table 3.7

Table 3.7: Single Layer Tracks Parameters

<b>Plate 3</b>						
# Track	Laser Power (W)	Speed (mm/min)	Laser Focus (mm)	Powder Flow Rate (rpm)	Z-step (%)	Deposition Strategy
7	750	700	6.5	6	25	Monodirectional
8	750	700	6.5	6	50	Monodirectional
9	750	700	6.5	6	75	Monodirectional
10	850	700	6.5	6	25	Monodirectional
11	850	700	6.5	6	50	Monodirectional
12	850	700	6.5	6	75	Monodirectional
13	750	700	6.5	6	25	Bidirectional
14	750	700	6.5	6	50	Bidirectional
15	750	700	6.5	6	75	Bidirectional
16	850	700	6.5	6	25	Bidirectional
17	850	700	6.5	6	50	Bidirectional
18	850	700	6.5	6	75	Bidirectional

The plate (same as Single Layer analysis) “Figure 3.20” is a 110×110×8,5mm<sup>3</sup> made of Ti64, with 4 holes for fixing it to the table.

### 3.3.2 Microscope Analysis

The parts have been prepared according to “Error! Reference source not found. Error! Reference source not found.”.

- **Top view analysis**

In “Figure 3.23” & “Figure 3.24”, the top-view photos are reported. The photos are obtained with the stereo microscope at different resolutions (1× and 3×). All tracks have been successfully deposited. No big differences are noted between the 12 wall tracks from this perspective.

		Focus 6,5 FeedRate 6 RPM	Z-Step 25%	Z-step 50%	Z-step 75%
Microscope Magnitude Monodirectional 1x	700 mm/min 750 W				
	700 mm/min 850 W				
Microscope Magnitude Monodirectional 3x	700 mm/min 750 W				
	700 mm/min 850 W				

Figure 3.23: Top View of Tracks 7 to 12 for single wall analysis

		Focus 6,5 FeedRate 6 RPM	Z-Step 25%	Z-step 50%	Z-step 75%
Microscope Magnitude Bidirectional 1x	700 mm/min 750 W				
	700 mm/min 850 W				
Microscope Magnitude Bidirectional 3x	700 mm/min 750 W				
	700 mm/min 850 W				

Figure 3.24: Top View of Tracks 13 to 18 for single wall analysis

In “Figure 3.25”, the cross-section of all the wall tracks and dimensions related to Table 3.8 are reported too. The dimensions were obtained with an optical microscope, and dimensions were evaluated with ImageJ.

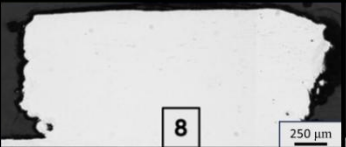
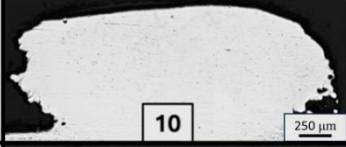
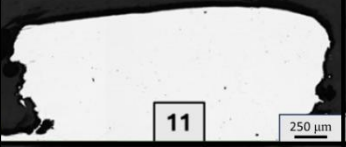
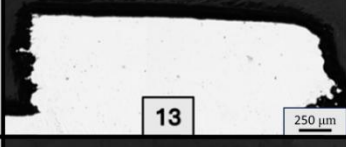
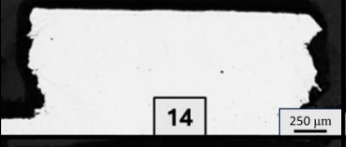
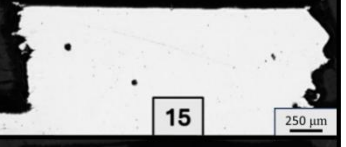
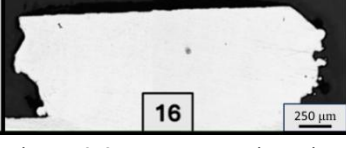
Focus 6,5 FeedRate 6 RPM	Z-Step 25%	Z-step 50%	Z-step 75%
700 mm/min 750 W	 7 250 μm	 8 250 μm	 9 250 μm
700 mm/min 850 W	 10 250 μm	 11 250 μm	 12 250 μm
700 mm/min 750 W	 13 250 μm	 14 250 μm	 15 250 μm
700 mm/min 850 W	 16 250 μm	 17 250 μm	 18 250 μm

Figure 3.25: Cross Section view of tracks 7 to 18 for single wall analysis.

Table 3.8: Wall Track dimension

# Track	Width [mm]	Height [mm]	Ratio W/H
7	1942	909	2.14
8	2105	1014	2.08
9	1919	920	2.09
10	1976	951	2.08
11	1998	993	2.01
12	2088	955	2.19
13	1962	772	2.54
14	1973	802	2.46
15	1895	748	2.53
16	2026	835	2.43
17	2155	828	2.60
18	2146	755	2.84

From data is possible to notice the following:

- With a bidirectional deposition (tracks 13-18), the overall height reached is lower than the monodirectional deposition. Even if it is not always possible to set a directional or bidirectional deposition, when parts are manufactured, a time case study should be done to analyze how much time is saved with a bidirectional strategy, and how much time is saved with a monodirectional one, considering that this latter guarantee higher tracks than the first ones.
- Since the number of layers is the same for each track, the expected result is that for a set of 3 tracks, the height will raise, but considering the following tracks:
  - o 7-9 at 75% Z-step, the height doesn't raise, and a decrease increase in width is shown with respect to 50% Z-step
  - o 10-12 at 75% Z-step, the height doesn't raise and an increase in width is shown
  - o 13-15 at 75% Z-step, the height doesn't raise and a decrease in width is shown with respect to 50% Z-step
  - o 16-18 at 75% Z-step, the height doesn't raise, and the width is constant with respect to tracks 16 and 17
- As the last state, the increase to 75% Z-step will have no benefits since the height of the material is not growing, meaning a possible loss of material during deposition and an incorrect adhesion between the two following layers.
- No big differences are shown between 25% and 50% Z-steps, with an increase both in width and in height for the 50% Z-steps. It is possible to notice that the lateral shape at 25% start to be rounded; this could create a non-straight wall during full-part deposition. Instead, in the 50% cross-section the shape is more linear and straight. The 50% Z-steps guarantee a time saving and a cost saving from a manufacturing point of view with less possibility to have shape deformation at the end of the deposition.

Based on the previous, the 50% Z-steps is the best choice for the parts building.

- **Parameters for Cube Creation**

As for previous paragraphs, the two combinations of parameters chosen for the next steps are the following:

# Track	Laser Power (W)	Speed (mm/min)	Laser Focus (mm)	powder flow rate (g/min)	Z-step (%)
8-14	750	700	6.5	10.25	50
11-17	850	700	6.5	10.25	50

### 3.4 Part Sample Production

2 sets of parameters have been selected for samples production. 6 cubes in total have been realized.

Table 3.9: Parameters for cube creation

# Cubes	Laser Power (W)	Speed (mm/min)	Laser Focus (mm)	powder flow rate (g/min)	Hatching (%)	Z-step (%)
1-3	750	700	6.5	10.25	50	50
4-6	850	700	6.5	10.25	50	50

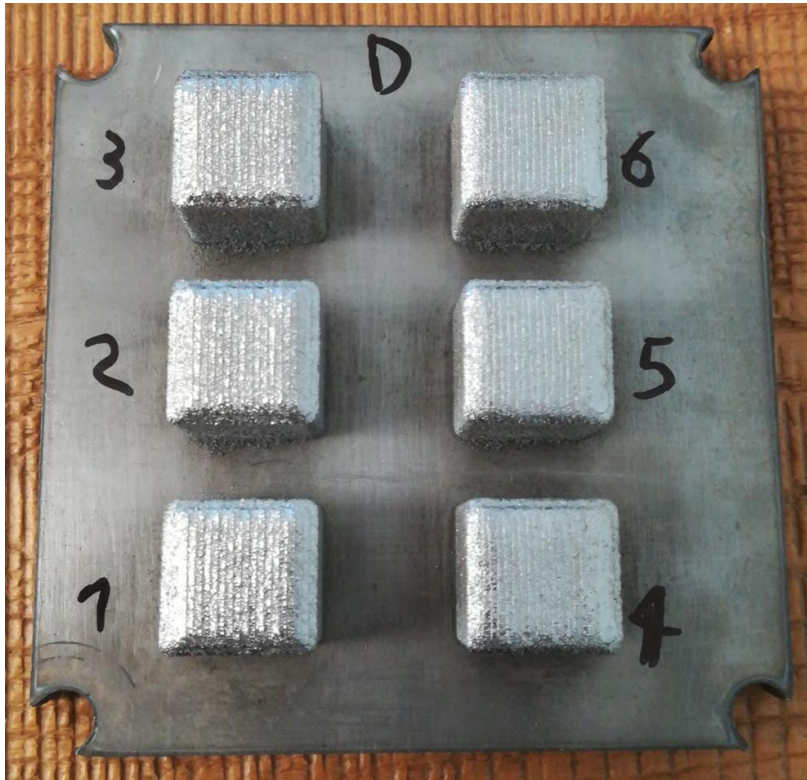


Figure 3.26: Plate with cubes

#### 3.4.1 Cross Section Analysis

After cube preparation, cutting, and polishing according to “Chapter 2 - Materials and Methods” the cross-section analysis was performed by taking 9 photos for each cube.

A schematic representation of the section zone is reported in “Figure 3.27”. The nomenclature of the section zone is then kept for the following paragraph as a reference system.

# Cube Section Scheme

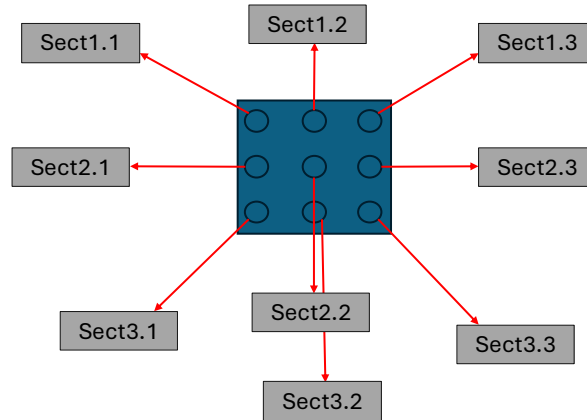


Figure 3.27: Schematic Representation of Cube section Zone

From “*Figure 3.28*” to “*Figure 3.33*”, all the cross-section images are reported. From these, the porosity has been analysed through the ImageJ program and reported in each figure.

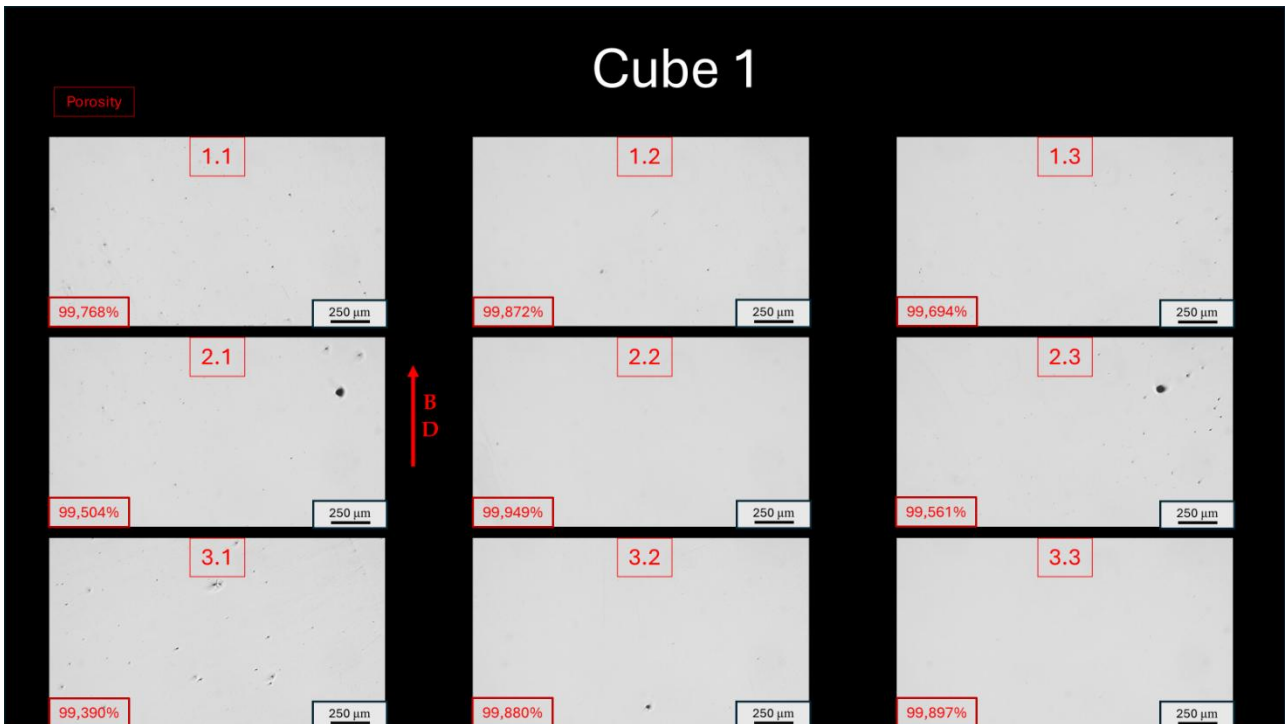


Figure 3.28: images of Cube 1 from optical microscope, superficial porosity calculated through ImageJ

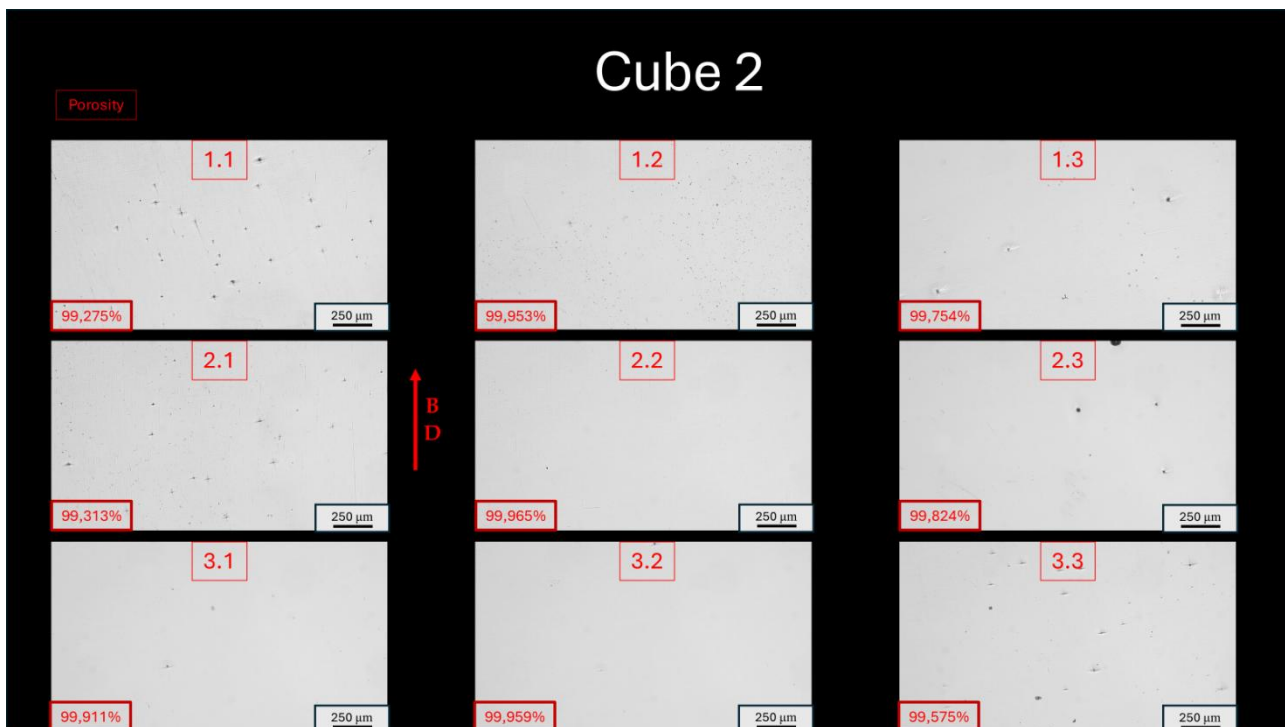


Figure 3.29: images of Cube 2 from optical microscope, superficial porosity calculated through ImageJ

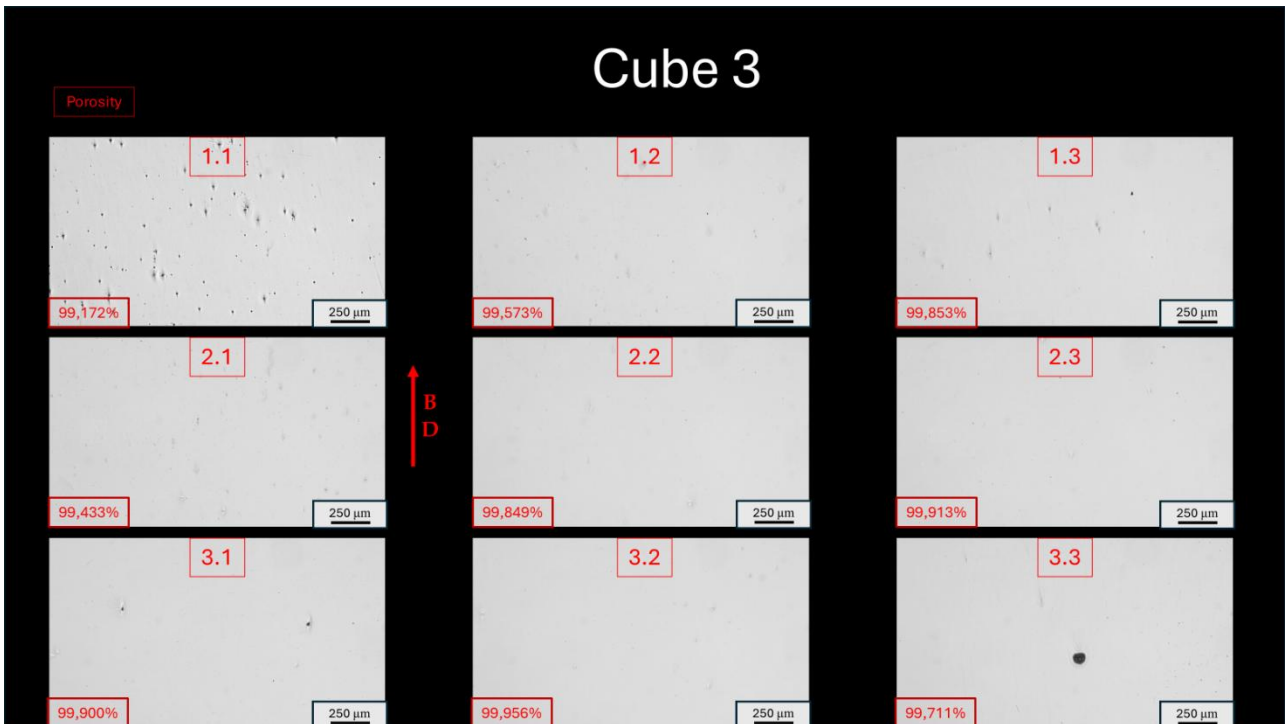


Figure 3.30: images of Cube 3 from optical microscope, superficial porosity calculated through ImageJ

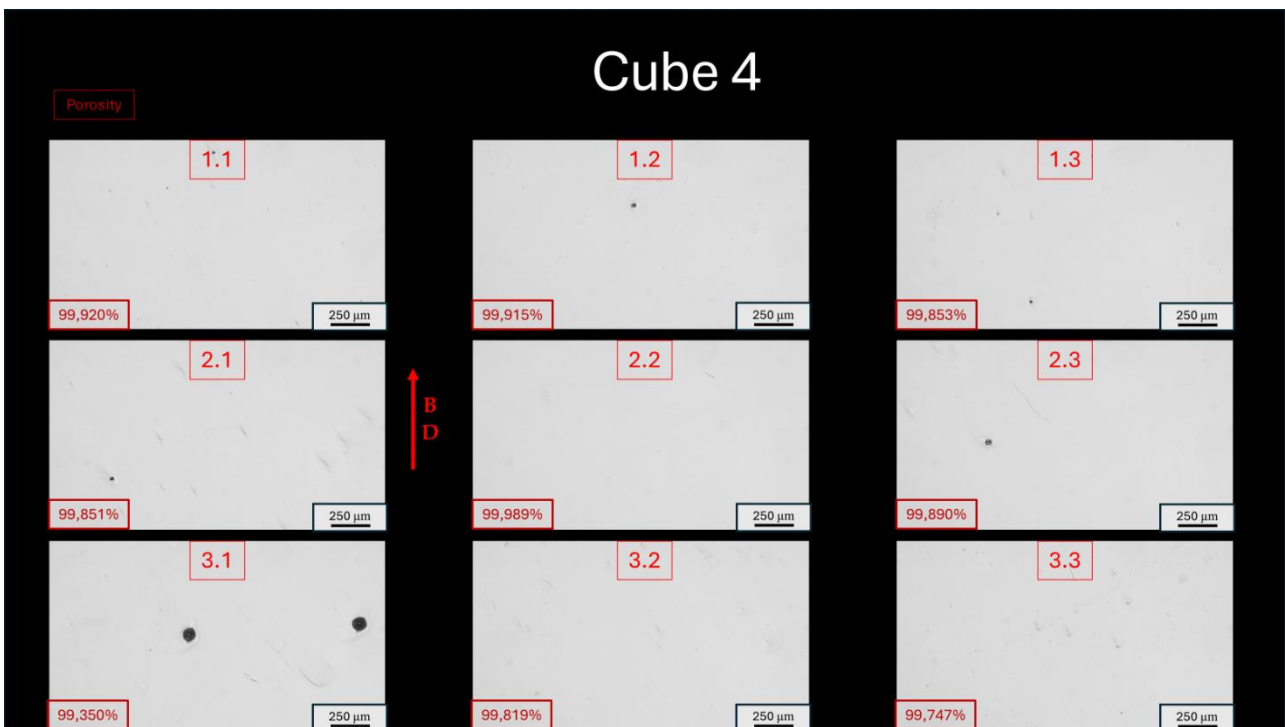


Figure 3.31: images of Cube 4 from optical microscope, superficial porosity calculated through ImageJ

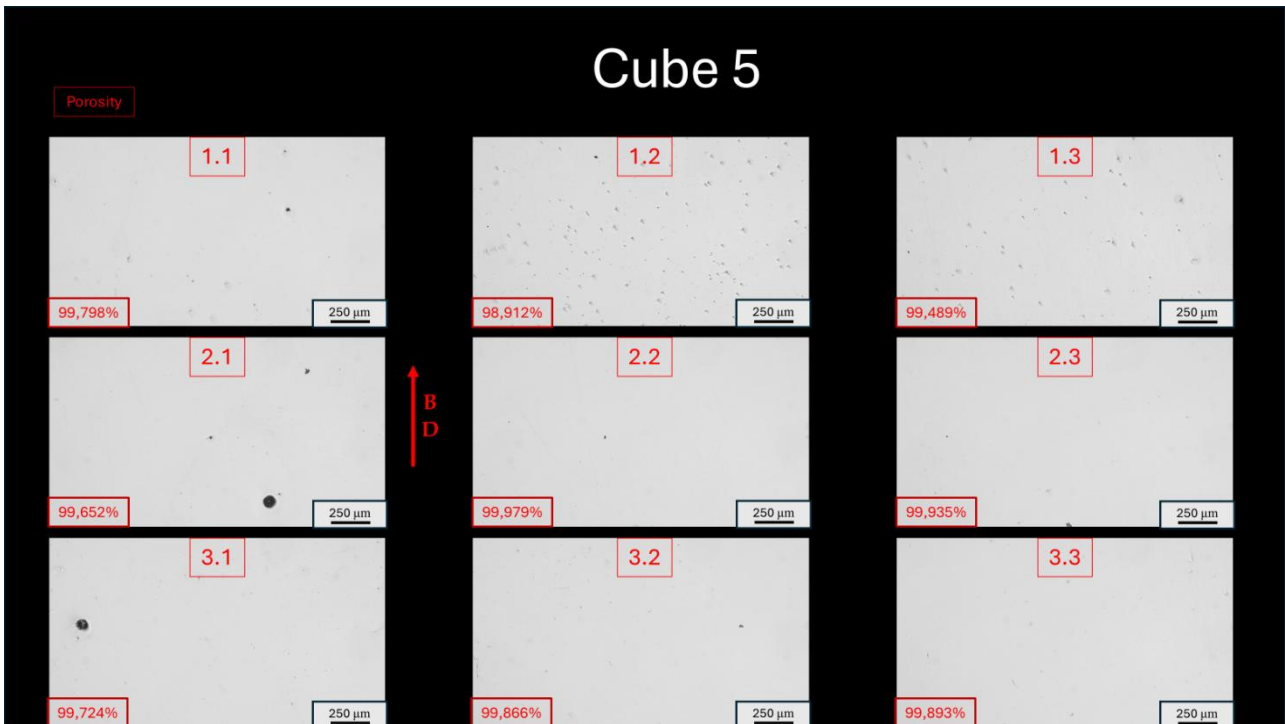


Figure 3.32: images of Cube 5 from optical microscope, superficial porosity calculated through ImageJ

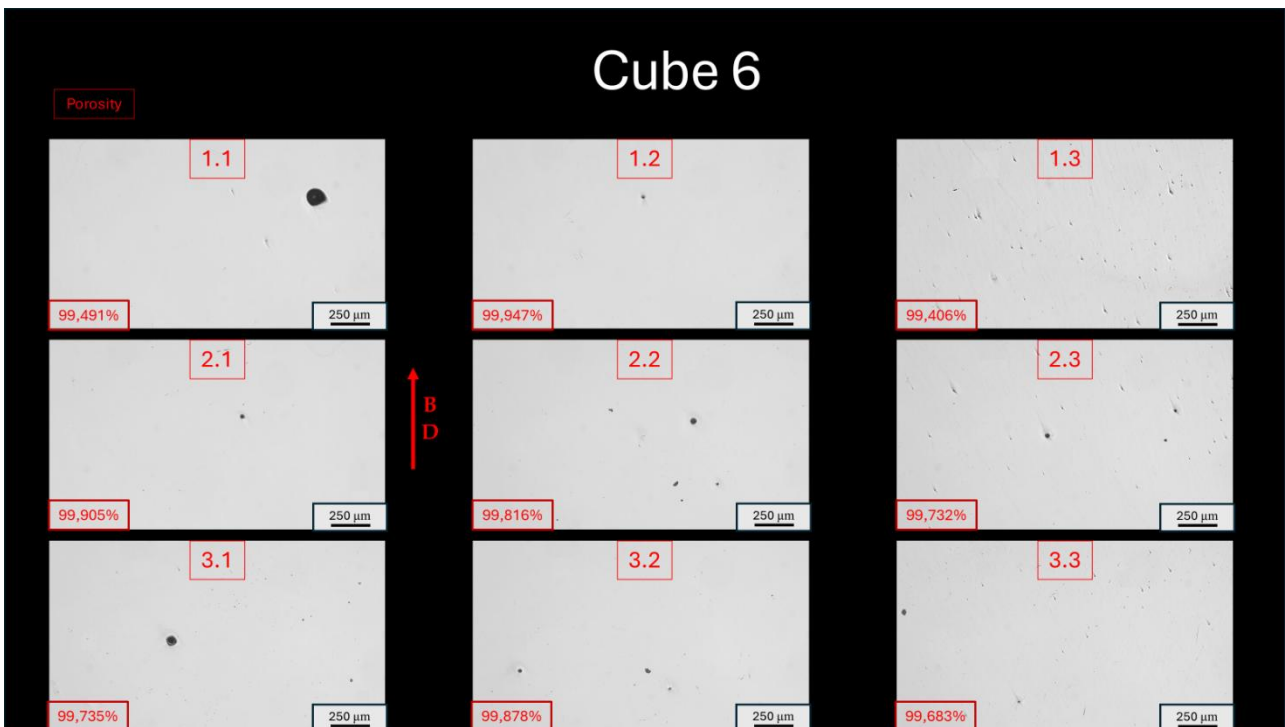


Figure 3.33: images of Cube 6 from optical microscope, superficial porosity calculated through ImageJ

To have an easier overview, all porosity data has been also summarized in *Table 3.10*.

Table 3.10: Summary of all superficial porosity of Cubes

	Cube1	Cube2	Cube3	Cube4	Cube5	Cube6
	99.77%	99.28%	99.17%	99.92%	99.80%	99.49%
	99.87%	98.95%	99.57%	99.92%	98.91%	99.95%
	99.69%	99.75%	99.85%	99.85%	99.49%	99.41%
	99.50%	99.31%	99.43%	99.85%	99.65%	99.91%
	99.95%	99.97%	99.85%	99.99%	99.98%	99.82%
	99.56%	99.82%	99.91%	99.89%	99.94%	99.73%
	99.39%	99.91%	99.90%	99.35%	99.72%	99.74%
	99.88%	99.96%	99.96%	99.82%	99.87%	99.88%
	99.90%	99.58%	99.71%	99.75%	99.89%	99.68%
Average	99.72%	99.61%	99.71%	99.81%	99.69%	99.73%
	99.68%			99.75%		

Based on the previous, it is possible to see that the resulting porosity from the cross-section analysis shows a high-density level of the parts, with minor differences between the two sets of parameters. In some case, example “*Figure 3.33 – 1.1*” some macro pores are still visible on the section. Due to the spherical shape, these are generated from gas inclusion in the parts during deposition. Anyway, a mean value of 99,5% is acceptable for mostly using services.

To have a wider overview of porosity and to cross-check the data found in the following section with tomography, the overall porosity of the cubes will be reported.

### 3.4.2 Tomography

One cube for each set of parameters was analyzed with tomograph. A representative photo is reported in “Figure 3.34” & “Figure 3.36” as well as Volume vs Diameter of defects found in “Figure 3.35” & “Figure 3.37”.

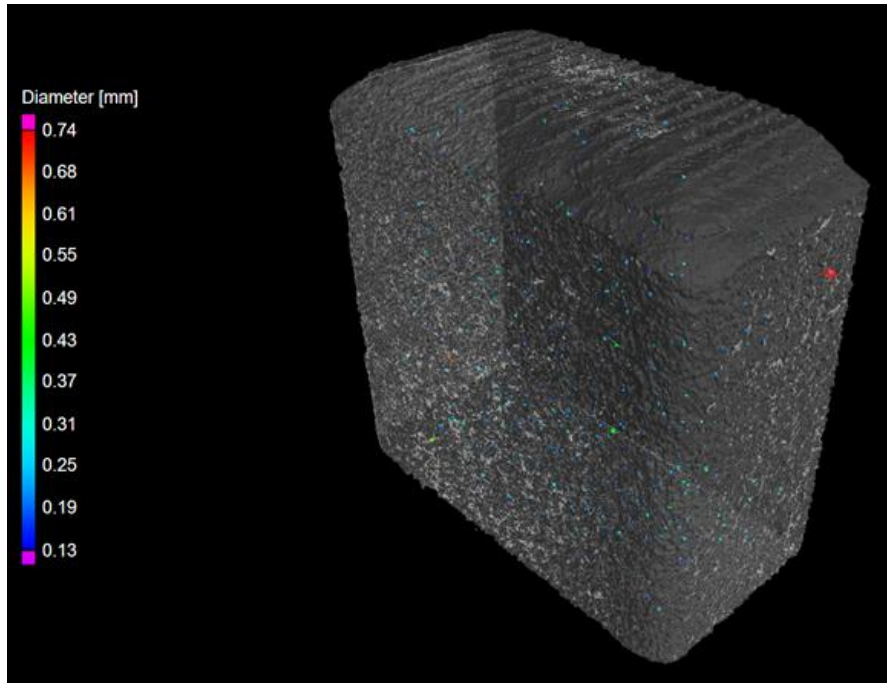


Figure 3.34: Cube 1 Tomography

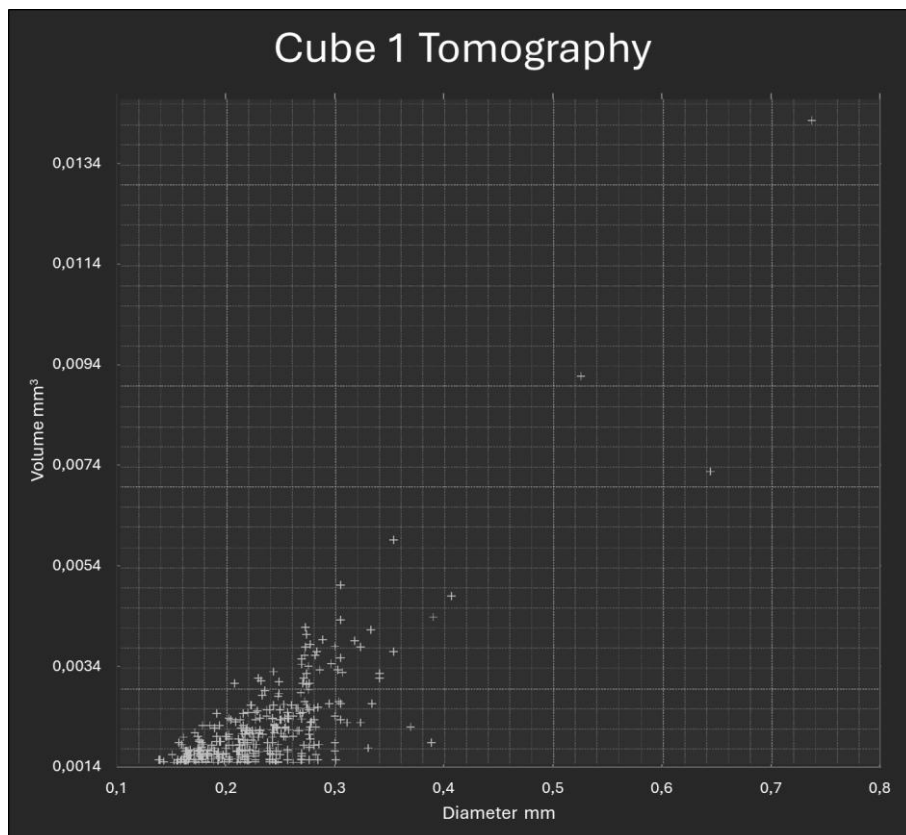


Figure 3.35: Diameter vs Volume of pores in Cube 1

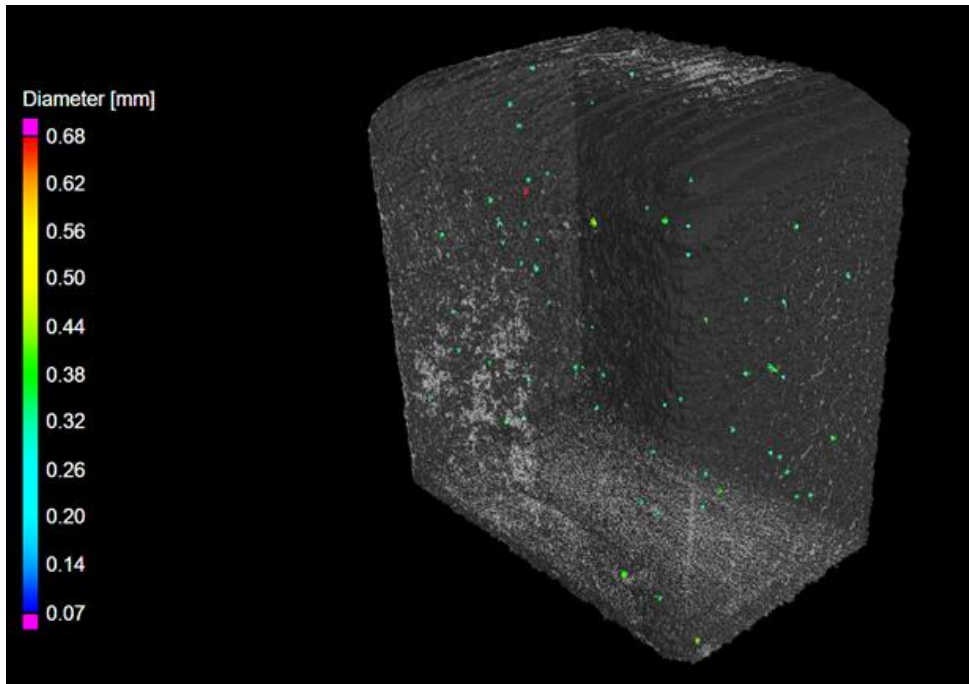


Figure 3.36: Cube 4 Tomography

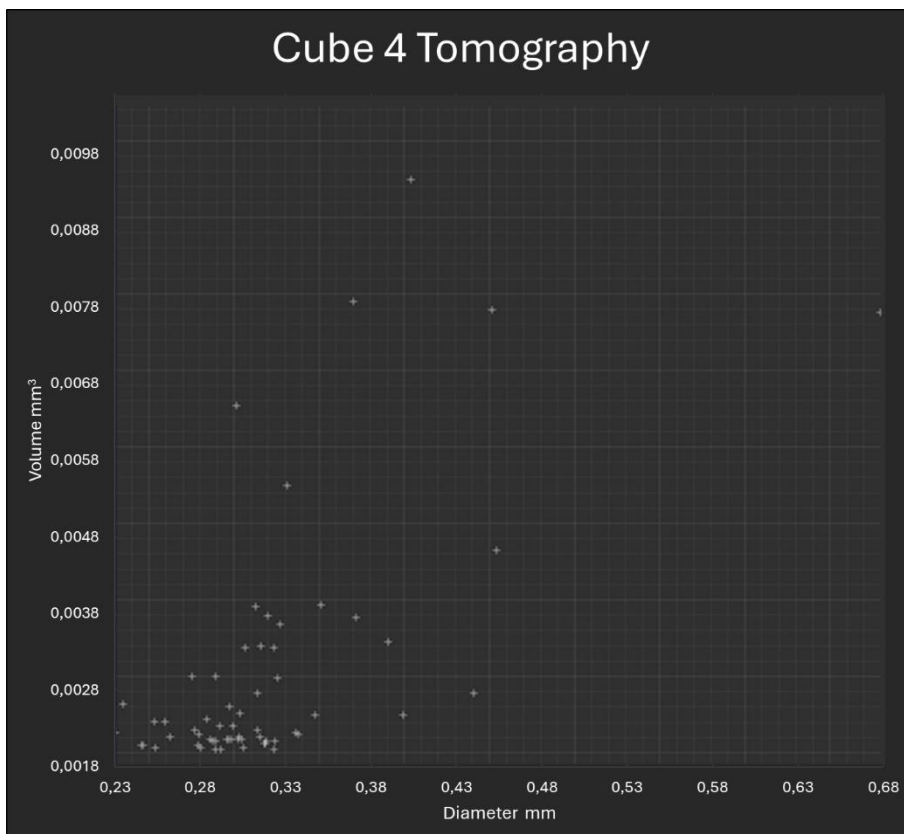


Figure 3.37: Diameter vs Volume of pores in Cube 4

The final results are summarized in “*Table 3.11*” as follows:

Table 3.11: Tomography Data Summary

	Cube 1	Cube 4
Material Volume [mm <sup>3</sup> ]	3805.19	4997.82
Defect Volume [mm <sup>3</sup> ]	0.42	0.19
Ratio [%}	0.011 %	0.004

The high level of density shown in the previous paragraph is confirmed by tomography, with a low level of porosity for the set of parameters. Also, in the tomography results, the set of parameters of cubes 4, 5, and 6 have a slightly lower porosity than the others. However, the difference in porosity is very low, and the density level is over 99,9% for each set of parameters. Due to the low statistical pool of data, both sets of parameters are considered acceptable for part production, for what concerns porosity.

Furthermore, the widest pores show a comparable diameter between the two sets of parameters, and even the distribution of volume – diameter is comparable between them.

### 3.4.3 Chemical etching

To highlight the microstructure of the parts, chemical etching was carried out on the cube cross-section according to “2.6 Chemical Hatching Process”. The cross-section surface results after *the etching process are shown in “Figure 2.1Figure 3.38” and in “Figure 3.39”*.

After chemical etching in “Figure 2.1Figure 3.38”, the photo was taken under a stereomicroscope. At this magnitude, it is possible to notice the contour strategy at the boundary. The horizontal shaded lines are the deposited layers, while the vertical ones are the grain main grain boundary.

At higher magnitude, “Figure 3.39”, the main grains are visible, and going to an even higher magnitude, it is possible to see the alpha grain boundary and alpha lamellae formed during cooling of the printed part.

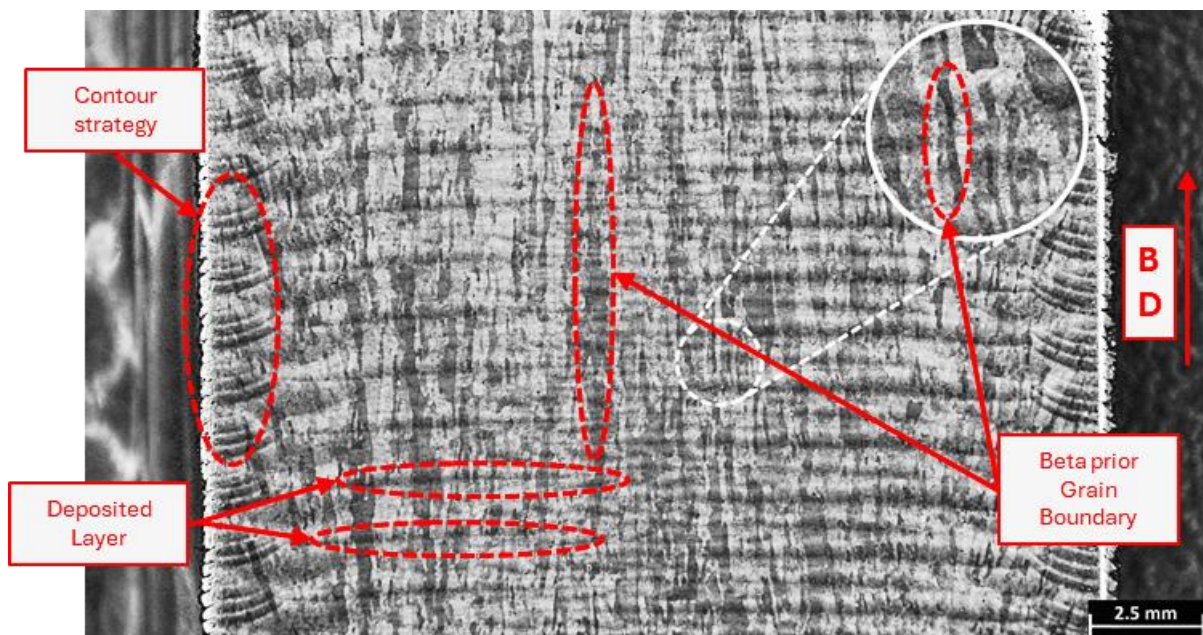


Figure 3.38: Cross section of the cube after etching chemical process, under stereomicroscope

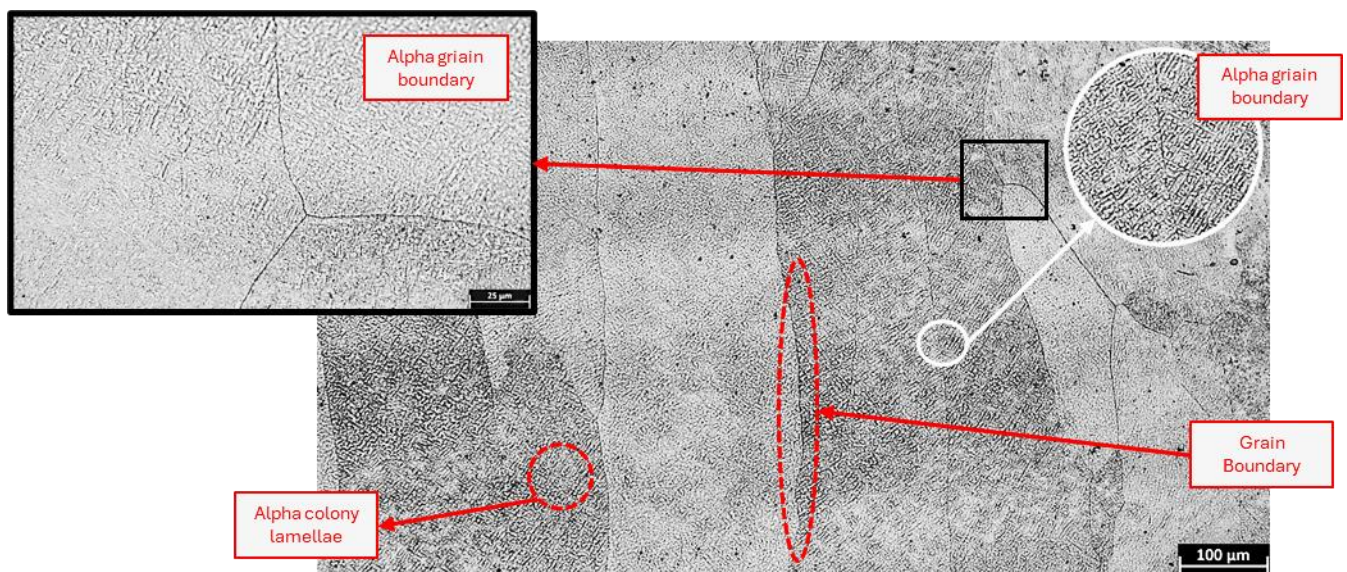


Figure 3.39: Cross section of the cube after etching chemical process, under optical microscope

### 3.4.4 Hardness Test

To have additional data to compare AM printed parts with conventional ones, a microhardness test was performed on the cross section. As for the previous paragraph, the schematic representation of the section zone is reported in “Figure 3.40”. The nomenclature of the section zone is then kept for the following paragraph as a reference system.

## Cube Section Scheme

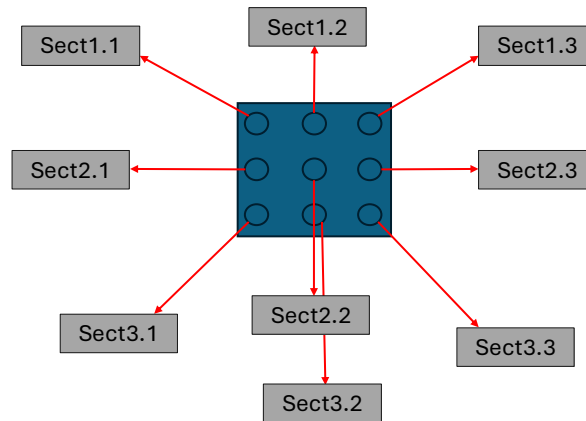


Figure 3.40: Schematic Representation of Cube section Zone

In Table 3.12, a summary of all the hardness values is reported. All values are in Vickers scale, they were measured with a load of 0.5 kgf and a dwell time of 15 s. Namely, all values are to be intended as HV0.5/15.

As it is possible to notice in the Table 3.12, no appreciable differences are present between the set of parameters of cubes 1 and 2 and cubes 4 and 5.

Furthermore, the values of hardness are comparable with respect to the hardness of traditional Titanium alloys, 350-450 HV.

Table 3.12: Microhardness test results

	<b>Cube 1</b>	<b>Cube 2</b>	<b>Cube 4</b>	<b>Cube 5</b>
<b>1.1</b>	388	368	390	365
<b>1.2</b>	384	365	385	361
<b>1.3</b>	386	366	388	362
<b>2.1</b>	378	362	381	359
<b>2.2</b>	375	360	378	358
<b>2.3</b>	383	364	380	360
<b>3.1</b>	372	357	371	355
<b>3.2</b>	368	355	367	351
<b>3.3</b>	374	356	375	353
Average	<b>378.7</b>	<b>361.4</b>	<b>379.4</b>	<b>358.2</b>
Total Average	<b>370,06</b>		<b>368.83</b>	
STD	<b>6.91</b>	<b>4.69</b>	<b>7.63</b>	<b>4.49</b>
Total STD	<b>5.80</b>		<b>6.06</b>	

## Chapter 4.

### Conclusion

The results show that with DED technology, it is possible to realize Ti6242 fully dense parts with the following set of parameters:

# Set	Laser Power (W)	Speed (mm/min)	Laser Focus (mm)	powder flow rate (g/min)	Hatching (%)	Z-step (%)
1	750	700	6.5	10.25	50	50
2	850	700	6.5	10.25	50	50

Throughout the process, it has been demonstrated that:

- Single Track Analysis is a reliable way to optimize in a cost-effective and short time solution the laser-related parameters as laser power, laser speed, laser Focus, and Powder Flow
- Single Wall and Single Layer Analysis is a reliable solution to optimize the strategy regarding xy-related and z-related parameters as hatching distance and z-step
- Cube creation is a sustainable way to validate the parameters found in the previous solution, as confirmed by tomography analysis for porosity.
- The Ti6242 creation through DED has shown minor differences with respect to traditional technology, as shown by microstructure analysis and hardness analysis.

The two sets of parameters show comparable porosity, comparable microhardness, and, during all the cross-section analysis, comparable cross-section. Both are considered a valid solution for printing Ti6242 in Borealis Cell.

The parameter optimization used is a sustainable, reliable, cost effective, and rapid implementation method to identify and optimize the parameters set to print a new material through an additive manufacturing process.

Further analysis could be performed in order to characterize the mechanical properties of the two sets of parameters and find the most suitable mechanical characteristics for the intended field of application.

## Bibliografy

- [1] Technical Committee AMT/8, *ISO/ASTM 52900:2021: additive manufacturing - general principle*.
- [2] M. Armstrong, H. Mehrabi, and N. Naveed, "An overview of modern metal additive manufacturing technology," *J Manuf Process*, vol. 84, pp. 1001–1029, 2022, doi: <https://doi.org/10.1016/j.jmapro.2022.10.060>.
- [3] W. Jamróz, J. Szafraniec, M. Kurek, and R. Jachowicz, "3D Printing in Pharmaceutical and Medical Applications – Recent Achievements and Challenges," *Pharm Res*, vol. 35, no. 9, p. 176, 2018, doi: 10.1007/s11095-018-2454-x.
- [4] B. Blakey-Milner *et al.*, "Metal additive manufacturing in aerospace: A review," *Mater Des*, vol. 209, p. 110008, 2021, doi: <https://doi.org/10.1016/j.matdes.2021.110008>.
- [5] A. Vafadar, F. Guzzomi, A. Rassau, and K. Hayward, "Advances in Metal Additive Manufacturing: A Review of Common Processes, Industrial Applications, and Current Challenges," *Applied Sciences*, vol. 11, no. 3, 2021, doi: 10.3390/app11031213.
- [6] Y. Kok *et al.*, "Anisotropy and heterogeneity of microstructure and mechanical properties in metal additive manufacturing: A critical review," *Mater Des*, vol. 139, pp. 565–586, 2018, doi: <https://doi.org/10.1016/j.matdes.2017.11.021>.
- [7] A. I. Nurhuda, S. Supriadi, Y. Whulanza, and A. S. Saragih, "Additive manufacturing of metallic based on extrusion process: A review," *J Manuf Process*, vol. 66, pp. 228–237, 2021, doi: <https://doi.org/10.1016/j.jmapro.2021.04.018>.
- [8] J. Gonzalez-Gutierrez, S. Cano, S. Schuschnigg, C. Kukla, J. Sapkota, and C. Holzer, "Additive Manufacturing of Metallic and Ceramic Components by the Material Extrusion of Highly-Filled Polymers: A Review and Future Perspectives," *Materials*, vol. 11, no. 5, 2018, doi: 10.3390/ma11050840.
- [9] Y. Zhang *et al.*, "Additive Manufacturing of Metallic Materials: A Review," *J Mater Eng Perform*, vol. 27, no. 1, pp. 1–13, 2018, doi: 10.1007/s11665-017-2747-y.
- [10] M. Ziaee and N. B. Crane, "Binder jetting: A review of process, materials, and methods," *Addit Manuf*, vol. 28, pp. 781–801, 2019, doi: <https://doi.org/10.1016/j.addma.2019.05.031>.
- [11] M. Ziaee and N. B. Crane, "Binder jetting: A review of process, materials, and methods," *Addit Manuf*, vol. 28, pp. 781–801, 2019, doi: <https://doi.org/10.1016/j.addma.2019.05.031>.
- [12] S. Mirzababaei and S. Pasebani, "A Review on Binder Jet Additive Manufacturing of 316L Stainless Steel," *Journal of Manufacturing and Materials Processing*, vol. 3, no. 3, 2019, doi: 10.3390/jmmp3030082.

- [13] S. Vock, B. Klöden, A. Kirchner, T. Weißgärber, and B. Kieback, "Powders for powder bed fusion: a review," *Progress in Additive Manufacturing*, vol. 4, no. 4, pp. 383–397, 2019, doi: 10.1007/s40964-019-00078-6.
- [14] A. Raza *et al.*, "Degradation of AlSi10Mg powder during laser based powder bed fusion processing," *Mater Des*, vol. 198, p. 109358, 2021, doi: <https://doi.org/10.1016/j.matdes.2020.109358>.
- [15] D. Kong *et al.*, "Microstructure and mechanical properties of nickel-based superalloy fabricated by laser powder-bed fusion using recycled powders," *International Journal of Minerals, Metallurgy and Materials*, vol. 28, no. 2, pp. 266–278, 2021, doi: 10.1007/s12613-020-2147-4.
- [16] A. Saboori, D. Gallo, S. Biamino, P. Fino, and M. Lombardi, "An Overview of Additive Manufacturing of Titanium Components by Directed Energy Deposition: Microstructure and Mechanical Properties," *Applied Sciences*, vol. 7, no. 9, 2017, doi: 10.3390/app7090883.
- [17] B. Dutta, "Directed Energy Deposition (DED) Technology," in *Encyclopedia of Materials: Metals and Alloys*, F. G. Caballero, Ed., Oxford: Elsevier, 2022, pp. 66–84. doi: <https://doi.org/10.1016/B978-0-12-819726-4.00035-1>.
- [18] B. Dutta, "Directed Energy Deposition (DED) Technology," in *Reference Module in Materials Science and Materials Engineering*, 2020. doi: 10.1016/B978-0-12-819726-4.00035-1.
- [19] D.-G. Ahn, "Directed Energy Deposition (DED) Process: State of the Art," *International Journal of Precision Engineering and Manufacturing-Green Technology*, vol. 8, no. 2, pp. 703–742, 2021, doi: 10.1007/s40684-020-00302-7.
- [20] A. Jiménez, P. Bidare, H. Hassanin, F. Tarlochan, S. Dimov, and K. Essa, "Powder-based laser hybrid additive manufacturing of metals: a review," *The International Journal of Advanced Manufacturing Technology*, vol. 114, no. 1, pp. 63–96, 2021, doi: 10.1007/s00170-021-06855-4.
- [21] U. M. Dilberoglu, B. Gharehpapagh, U. Yaman, and M. Dolen, "Current trends and research opportunities in hybrid additive manufacturing," *The International Journal of Advanced Manufacturing Technology*, vol. 113, no. 3, pp. 623–648, 2021, doi: 10.1007/s00170-021-06688-1.
- [22] B. Zheng *et al.*, "On the evolution of microstructure and defect control in 316L SS components fabricated via directed energy deposition," *Materials Science and Engineering: A*, vol. 764, p. 138243, 2019, doi: <https://doi.org/10.1016/j.msea.2019.138243>.

- [23] M. Liu, A. Kumar, S. Bukkapatnam, and M. Kuttolamadom, "A Review of the Anomalies in Directed Energy Deposition (DED) Processes & Potential Solutions - Part Quality & Defects," *Procedia Manuf*, vol. 53, pp. 507–518, 2021, doi: <https://doi.org/10.1016/j.promfg.2021.06.093>.
- [24] "Prima Additive ." Accessed: Feb. 02, 2025. [Online]. Available: <https://www.primaadditive.com/en/technologies/direct-energy-deposition>
- [25] "Optomec." Accessed: Feb. 02, 2025. [Online]. Available: <https://optomec.com/3d-printed-metals/lens-printers/>
- [26] "DM3D Technology." Accessed: Feb. 02, 2025. [Online]. Available: <https://dm3dtech.com/>
- [27] "Prima Additive PBF." Accessed: Feb. 02, 2025. [Online]. Available: <https://www.primaadditive.com/en/technologies/powder-bed-fusion>
- [28] "EOS." Accessed: Feb. 02, 2025. [Online]. Available: [https://www.eos.info/it/chisiamo/cosafacciamo/dmls?utm\\_term=&utm\\_campaign=%5Bwyn%5D+Generic+%5BEMEA%5D+%5BPMMax%5D&utm\\_source=adwords&utm\\_medium=ppc&hsa\\_acc=3851378066&hsa\\_cam=21234802769&hsa\\_grp=&hsa\\_ad=&hsa\\_src=x&hsa\\_tgt=&hsa\\_kw=&hsa\\_mt=&hsa\\_net=adwords&hsa\\_ver=3&gad\\_source=1&gclid=CjwKCAiAzPy8BhBoEiwAbnM9O-F6X2rkDsLzDyYysVa7KtN68i8qD-yUVhKW6JHBRyxBFbzYZaopPhoCJpMQAvD\\_BwE](https://www.eos.info/it/chisiamo/cosafacciamo/dmls?utm_term=&utm_campaign=%5Bwyn%5D+Generic+%5BEMEA%5D+%5BPMMax%5D&utm_source=adwords&utm_medium=ppc&hsa_acc=3851378066&hsa_cam=21234802769&hsa_grp=&hsa_ad=&hsa_src=x&hsa_tgt=&hsa_kw=&hsa_mt=&hsa_net=adwords&hsa_ver=3&gad_source=1&gclid=CjwKCAiAzPy8BhBoEiwAbnM9O-F6X2rkDsLzDyYysVa7KtN68i8qD-yUVhKW6JHBRyxBFbzYZaopPhoCJpMQAvD_BwE)
- [29] "Nikon SLM." Accessed: Feb. 02, 2025. [Online]. Available: <https://nikon-slm-solutions.com/slm-systems/>
- [30] "GE calibrium." Accessed: Feb. 02, 2025. [Online]. Available: <https://www.colibriumadditive.com/>
- [31] M. Koike *et al.*, "Evaluation of Titanium Alloys Fabricated Using Rapid Prototyping Technologies—Electron Beam Melting and Laser Beam Melting," *Materials*, vol. 4, no. 10, pp. 1776–1792, 2011, doi: 10.3390/ma4101776.
- [32] H. D. Nguyen *et al.*, "A critical review on additive manufacturing of Ti-6Al-4V alloy: microstructure and mechanical properties," *Journal of Materials Research and Technology*, vol. 18, pp. 4641–4661, 2022, doi: <https://doi.org/10.1016/j.jmrt.2022.04.055>.
- [33] K. Kim, K. Park, H. W. Jeon, and G. E. Kremer, "Design complexity based flexible order dispatching for additive manufacturing production," *Int J Prod Econ*, vol. 274, p. 109307, 2024, doi: <https://doi.org/10.1016/j.ijpe.2024.109307>.

- [34] C. Prakash, S. Singh, H. Kopperi, S. Ramakrihna, and S. V. Mohan, "Comparative job production based life cycle assessment of conventional and additive manufacturing assisted investment casting of aluminium: A case study," *J Clean Prod*, vol. 289, p. 125164, 2021, doi: <https://doi.org/10.1016/j.jclepro.2020.125164>.
- [35] N. Midrez, A. Siddiqi, G. Mercusot, and B. Cameron, "Evaluating the environmental and financial performance of additive manufacturing at scale in the consumer goods industry," *Sustain Prod Consum*, vol. 52, pp. 580–601, 2024, doi: <https://doi.org/10.1016/j.spc.2024.11.013>.
- [36] L. Kang, J. Jin, X. Liu, and H. Chen, "Effects of surface roughness on mechanical properties of laser-cladding additively manufactured 316L stainless steel sheets," *J Constr Steel Res*, vol. 224, p. 109136, 2025, doi: <https://doi.org/10.1016/j.jcsr.2024.109136>.
- [37] M. A. Kumar, J. C. Nieto-Fuentes, and J. A. Rodríguez-Martínez, "Impact of surface roughness on the formation of necking instabilities in additive manufactured porous metal plates subjected to dynamic plane strain stretching," *Finite Elements in Analysis and Design*, vol. 242, p. 104275, 2024, doi: <https://doi.org/10.1016/j.finel.2024.104275>.
- [38] F. Fan, S. Jalui, K. Shahed, B. Mullany, and G. Manogharan, "Mass finishing for additive manufacturing: Tribological analysis, surface topology, image processing, predictive model, and processing recommendations," *Tribol Int*, vol. 204, p. 110486, 2025, doi: <https://doi.org/10.1016/j.triboint.2024.110486>.
- [39] M. Tyburec, M. Doškář, M. Somr, M. Kružík, and J. Zeman, "Modular-topology optimization for additive manufacturing of reusable mechanisms," *Comput Struct*, vol. 307, p. 107630, 2025, doi: <https://doi.org/10.1016/j.compstruc.2024.107630>.
- [40] K. C. G. Candioto, L. F. Moretao, and B. S. Linke, "Mass finishing of additively manufactured AISI 316L using pecan nutshells as sustainable abrasive media," *Manuf Lett*, vol. 41, pp. 1645–1651, 2024, doi: <https://doi.org/10.1016/j.mfglet.2024.09.191>.
- [41] A. Al Rashid and M. Koç, "Additive manufacturing for sustainability, circularity and zero-waste: 3DP products from waste plastic bottles," *Composites Part C: Open Access*, vol. 14, p. 100463, 2024, doi: <https://doi.org/10.1016/j.jcomc.2024.100463>.
- [42] S. Karadayi-Usta, "Sustainable additive manufacturing supply chains with a plithogenic stakeholder analysis: Waste reduction through digital transformation," *CIRP J Manuf Sci Technol*, vol. 55, pp. 261–271, 2024, doi: <https://doi.org/10.1016/j.cirpj.2024.10.004>.
- [43] C. Suwanpreecha and A. Manonukul, "On the build orientation effect in as-printed and as-sintered bending properties of 17-4PH alloy fabricated by metal fused

filament fabrication," *Rapid Prototyp J*, vol. ahead-of-print, Jan. 2022, doi: 10.1108/RPJ-07-2021-0174.

- [44] T. Kurose *et al.*, "Influence of the Layer Directions on the Properties of 316L Stainless Steel Parts Fabricated through Fused Deposition of Metals," *Materials*, vol. 13, no. 11, 2020, doi: 10.3390/ma13112493.
- [45] C. Guo *et al.*, "Effect of processing parameters on surface roughness, porosity and cracking of as-built IN738LC parts fabricated by laser powder bed fusion," *J Mater Process Technol*, vol. 285, p. 116788, 2020, doi: <https://doi.org/10.1016/j.jmatprotec.2020.116788>.
- [46] A. Oleff, B. Küster, M. Stonis, and L. Overmeyer, "Process monitoring for material extrusion additive manufacturing: a state-of-the-art review," *Progress in Additive Manufacturing*, vol. 6, no. 4, pp. 705–730, 2021, doi: 10.1007/s40964-021-00192-4.
- [47] M. C. Brennan, J. S. Keist, and T. A. Palmer, "Defects in Metal Additive Manufacturing Processes," *J Mater Eng Perform*, vol. 30, no. 7, pp. 4808–4818, 2021, doi: 10.1007/s11665-021-05919-6.
- [48] B. C. Lam, C. T. Kassner, J. W. Kemp, B. T. Leicht, B. T. Bohan, and L. M. Rueschhoff, "Delamination mitigation in additively manufactured Al<sub>2</sub>O<sub>3</sub> via enhanced thermal postprocessing," *Int J Appl Ceram Technol*, vol. 21, no. 2, pp. 675–685, Mar. 2024, doi: <https://doi.org/10.1111/ijac.14572>.
- [49] Z. Liu, C. Ma, Z. Chang, P. Yan, and F. Li, "Advances in crack formation mechanism and inhibition strategy for ceramic additive manufacturing," *J Eur Ceram Soc*, vol. 43, no. 12, pp. 5078–5098, 2023, doi: <https://doi.org/10.1016/j.jeurceramsoc.2023.05.008>.
- [50] J. C. Hastie, M. E. Kartal, L. N. Carter, M. M. Attallah, and D. M. Mulvihill, "Classifying shape of internal pores within AlSi10Mg alloy manufactured by laser powder bed fusion using 3D X-ray micro computed tomography: Influence of processing parameters and heat treatment," *Mater Charact*, vol. 163, p. 110225, 2020, doi: <https://doi.org/10.1016/j.matchar.2020.110225>.
- [51] R. Snell *et al.*, "Methods for Rapid Pore Classification in Metal Additive Manufacturing," *JOM*, vol. 72, no. 1, pp. 101–109, 2020, doi: 10.1007/s11837-019-03761-9.
- [52] Z. Liu, B. He, T. Lyu, and Y. Zou, "A Review on Additive Manufacturing of Titanium Alloys for Aerospace Applications: Directed Energy Deposition and Beyond Ti-6Al-4V," *JOM*, vol. 73, no. 6, pp. 1804–1818, 2021, doi: 10.1007/s11837-021-04670-6.
- [53] B. Dutta and F. H. Froes, "Chapter 1 - The Additive Manufacturing of Titanium Alloys," in *Additive Manufacturing of Titanium Alloys*, B. Dutta and F. H. Froes, Eds.,

Butterworth-Heinemann, 2016, pp. 1–10. doi: <https://doi.org/10.1016/B978-0-12-804782-8.00001-X>.

- [54] R. P. Kolli and A. Devaraj, "A Review of Metastable Beta Titanium Alloys," *Metals (Basel)*, 2018, [Online]. Available: <https://api.semanticscholar.org/CorpusID:102340650>
- [55] A. Carrozza, A. Aversa, P. Fino, and M. Lombardi, "A study on the Microstructure and Mechanical Properties of the Ti-6Al-2Sn-4Zr-6Mo Alloy Produced via Laser Powder Bed Fusion," *J Alloys Compd*, vol. 870, p. 159329, Aug. 2021, doi: 10.1016/j.jallcom.2021.159329.
- [56] Z. Guo, S. Malinov, and W. Sha, "Modelling beta transus temperature of titanium alloys using artificial neural network," *Comput Mater Sci*, vol. 32, no. 1, pp. 1–12, 2005, doi: <https://doi.org/10.1016/j.commatsci.2004.05.004>.
- [57] Y. Zhu, X. Tian, J. Li, and H. Wang, "Microstructure evolution and layer bands of laser melting deposition Ti-6.5Al-3.5Mo-1.5Zr-0.3Si titanium alloy," *J Alloys Compd*, vol. 616, pp. 468–474, 2014, doi: <https://doi.org/10.1016/j.jallcom.2014.07.161>.
- [58] Z. Liu, B. He, T. Lyu, and Y. Zou, "A Review on Additive Manufacturing of Titanium Alloys for Aerospace Applications: Directed Energy Deposition and Beyond Ti-6Al-4V," *JOM*, vol. 73, Aug. 2021, doi: 10.1007/s11837-021-04670-6.
- [59] N. A. Kistler, D. J. Corbin, A. R. Nassar, E. W. Reutzler, and A. M. Beese, "Effect of processing conditions on the microstructure, porosity, and mechanical properties of Ti-6Al-4V repair fabricated by directed energy deposition," *J Mater Process Technol*, vol. 264, pp. 172–181, 2019, doi: <https://doi.org/10.1016/j.jmatprotec.2018.08.041>.
- [60] N. Sanaei and A. Fatemi, "Defect-based fatigue life prediction of L-PBF additive manufactured metals," *Eng Fract Mech*, vol. 244, p. 107541, 2021, doi: <https://doi.org/10.1016/j.engfracmech.2021.107541>.
- [61] P. Åkerfeldt, R. Pederson, and M.-L. Antti, "A fractographic study exploring the relationship between the low cycle fatigue and metallurgical properties of laser metal wire deposited Ti-6Al-4V," *Int J Fatigue*, vol. 87, pp. 245–256, 2016, doi: <https://doi.org/10.1016/j.ijfatigue.2016.02.011>.
- [62] A. S. M. I. H. Committee, *ASM handbook. Volume 2, Properties and selection: nonferrous alloys and special-purpose materials*, 10th ed. Materials Park, OH: ASM International, 1990. [Online]. Available: <http://app.knovel.com/web/toc.v/cid:kpASMHVP07>
- [63] C. Wang, F. Li, X. Meili, J. Dong, and J. Li, "Microstructures and Mechanical Properties of Ti-6Al-4V Alloy Processed by Multi-Process," *Rare Metal Materials and Engineering*, vol. 34, Aug. 2015, doi: 10.1016/S1875-5372(15)30059-X.

- [64] S. Rajan, P. Wanjara, J. Gholipour, and A. Kabir, "Fatigue Behavior of Linear Friction Welded Ti-6Al-4V and Ti-6Al-2Sn-4Zr-2Mo-0.1Si Dissimilar Welds," *Materials*, vol. 14, p. 3136, Aug. 2021, doi: 10.3390/ma14113136.
- [65] G. B. Viswanathan, K. Subramanian, R. W. Hayes, and M. J. Mills, "Creep behaviour of Ti-6Al-2Sn-4Zr-2Mo: II. Mechanisms of deformation," *Acta Mater*, vol. 50, Aug. 2002, doi: 10.1016/S1359-6454(02)00280-X.
- [66] H. Fan, C. Wang, Y. Tian, K. Zhou, and S. Yang, "Laser powder bed fusion (L-PBF) of Ti-6Al-4V/Ti-6Al-2Sn-4Zr-2Mo and Ti-6Al-4V/ $\gamma$ -TiAl bimetals: Processability, interface and mechanical properties," *Materials Science and Engineering: A*, vol. 871, p. 144907, 2023, doi: <https://doi.org/10.1016/j.msea.2023.144907>.
- [67] A. Perumal, A. Azhagurajan, S. Baskaran, R. Prithvirajan, and P. Narayansamy, "Statistical evaluation and performance analysis of electrical discharge machining (EDM) characteristics of hard Ti-6Al-2Sn-4Zr-2Mo alloy," *Mater Res Express*, vol. 6, no. 5, p. 056552, 2019, doi: 10.1088/2053-1591/ab06da.
- [68] C. Siemers, M. Bäker, F. Brunke, D. Wolter, and H. Sibus, "4.6 - Aluminum- and vanadium-free titanium alloys for application in medical engineering," in *Titanium in Medical and Dental Applications*, F. H. Froes and M. Qian, Eds., Woodhead Publishing, 2018, pp. 477–492. doi: <https://doi.org/10.1016/B978-0-12-812456-7.00021-4>.
- [69] X. Li, S. Siahpour, J. Lee, Y. Wang, and J. Shi, "Deep Learning-Based Intelligent Process Monitoring of Directed Energy Deposition in Additive Manufacturing with Thermal Images," *Procedia Manuf*, vol. 48, pp. 643–649, 2020, doi: <https://doi.org/10.1016/j.promfg.2020.05.093>.
- [70] D. R. Feenstra, A. Molotnikov, and N. Birbilis, "Utilisation of artificial neural networks to rationalise processing windows in directed energy deposition applications," *Mater Des*, vol. 198, p. 109342, 2021, doi: <https://doi.org/10.1016/j.matdes.2020.109342>.
- [71] Z. Zhu, K. Ferreira, N. Anwer, L. Mathieu, K. Guo, and L. Qiao, "Convolutional Neural Network for geometric deviation prediction in Additive Manufacturing," *Procedia CIRP*, vol. 91, pp. 534–539, 2020, doi: <https://doi.org/10.1016/j.procir.2020.03.108>.
- [72] J. Ertveldt, P. Guillaume, and J. Helsen, "MiCLAD as a platform for real-time monitoring and machine learning in laser metal deposition," *Procedia CIRP*, vol. 94, pp. 456–461, 2020, doi: <https://doi.org/10.1016/j.procir.2020.09.164>.
- [73] C. Zhong, T. Biermann, A. Gasser, and R. Poprawe, "Experimental study of effects of main process parameters on porosity, track geometry, deposition rate, and powder

efficiency for high deposition rate laser metal deposition," *J Laser Appl*, vol. 27, no. 4, p. 042003, Jul. 2015, doi: 10.2351/1.4923335.

- [74] G. Wang, X. Sun, M. Huang, Y. Qin, Y. Yao, and S. Yang, "Influence of processing parameters on the microstructure and tensile property of 85 W-15Ni produced by laser direct deposition," *Int J Refract Metals Hard Mater*, vol. 82, pp. 227–233, 2019, doi: <https://doi.org/10.1016/j.ijrmhm.2019.04.016>.
- [75] T. Durejko *et al.*, "Structure and properties of the Fe<sub>3</sub>Al-type intermetallic alloy fabricated by laser engineered net shaping (LENS)," *Materials Science and Engineering: A*, vol. 650, pp. 374–381, 2016, doi: <https://doi.org/10.1016/j.msea.2015.10.076>.
- [76] A. Reichardt *et al.*, "Development and characterization of Ti-6Al-4V to 304L stainless steel gradient components fabricated with laser deposition additive manufacturing," *Mater Des*, vol. 104, pp. 404–413, 2016, doi: <https://doi.org/10.1016/j.matdes.2016.05.016>.
- [77] K. Zhang, S. Wang, W. Liu, and X. Shang, "Characterization of stainless steel parts by Laser Metal Deposition Shaping," *Mater Des*, vol. 55, pp. 104–119, 2014, doi: <https://doi.org/10.1016/j.matdes.2013.09.006>.
- [78] T. S. S. K. Mitun Das Vamsi Krishna Balla and I. Manna, "Fabrication of Biomedical Implants using Laser Engineered Net Shaping (LENS™)," *Transactions of the Indian Ceramic Society*, vol. 72, no. 3, pp. 169–174, 2013, doi: 10.1080/0371750X.2013.851619.
- [79] Q. Chao, T. Guo, T. Jarvis, X. Wu, P. Hodgson, and D. Fabijanic, "Direct laser deposition cladding of Al<sub>x</sub>CoCrFeNi high entropy alloys on a high-temperature stainless steel," *Surf Coat Technol*, vol. 332, pp. 440–451, 2017, doi: <https://doi.org/10.1016/j.surfcoat.2017.09.072>.
- [80] Y. Yao, Y. Huang, B. Chen, C. Tan, Y. Su, and J. Feng, "Influence of processing parameters and heat treatment on the mechanical properties of 18Ni300 manufactured by laser based directed energy deposition," *Opt Laser Technol*, vol. 105, pp. 171–179, 2018, doi: <https://doi.org/10.1016/j.optlastec.2018.03.011>.
- [81] A. S. Kamran Shah Andrew J. Pinkerton and L. Li, "Effects of Melt Pool Variables and Process Parameters in Laser Direct Metal Deposition of Aerospace Alloys," *Materials and Manufacturing Processes*, vol. 25, no. 12, pp. 1372–1380, 2010, doi: 10.1080/10426914.2010.480999.
- [82] A. J. Pinkerton, "Advances in the modeling of laser direct metal deposition," *J Laser Appl*, vol. 27, no. S1, p. S15001, Dec. 2014, doi: 10.2351/1.4815992.
- [83] N. A. Kistler, A. R. Nassar, E. W. Reutzel, D. J. Corbin, and A. M. Beese, "Effect of directed energy deposition processing parameters on laser deposited Inconel® 718:

Microstructure, fusion zone morphology, and hardness," *J Laser Appl*, vol. 29, no. 2, p. 022005, Apr. 2017, doi: 10.2351/1.4979702.

- [84] J. L. Bennett, S. J. Wolff, G. Hyatt, K. Ehmann, and J. Cao, "Thermal effect on clad dimension for laser deposited Inconel 718," *J Manuf Process*, vol. 28, pp. 550–557, 2017, doi: <https://doi.org/10.1016/j.jmapro.2017.04.024>.
- [85] B. Bax, R. Rajput, R. Kellet, and M. Reisacher, "Systematic evaluation of process parameter maps for laser cladding and directed energy deposition," *Addit Manuf*, vol. 21, pp. 487–494, 2018, doi: <https://doi.org/10.1016/j.addma.2018.04.002>.
- [86] R. Sampson, R. Lancaster, M. Sutcliffe, D. Carswell, C. Hauser, and J. Barras, "The influence of key process parameters on melt pool geometry in direct energy deposition additive manufacturing systems," *Opt Laser Technol*, vol. 134, p. 106609, 2021, doi: <https://doi.org/10.1016/j.optlastec.2020.106609>.
- [87] Y. Han, W. Lu, T. Jarvis, J. Shurvinton, and X. Wu, "Investigation on the Microstructure of Direct Laser Additive Manufactured Ti6Al4V Alloy," *Materials Research*, vol. 18, no. suppl 1, pp. 24–28, Nov. 2015, doi: 10.1590/1516-1439.322214.